INVESTIGATION OF NUMERICAL SCHEMES AND THEIR EFFECTS ON IMPACT PRESSURES IN NUMERICAL MODELLING

A THESIS SUBMITTED TO
THE GRADUATE SCHOOL OF NATURAL AND APPLIED SCIENCES
OF
MIDDLE EAST TECHNICAL UNIVERSITY

BY

SEMİH BATUHAN ÇANDIR

IN PARTIAL FULFILLMENT OF THE REQUIREMENTS
FOR
THE DEGREE OF MASTER OF SCIENCE
IN
CIVIL ENGINEERING

FEBRUARY 2022

Approval of the thesis:

INVESTIGATION OF NUMERICAL SCHEMES AND THEIR EFFECTS ON IMPACT PRESSURES IN NUMERICAL MODELLING

submitted by **SEMİH BATUHAN ÇANDIR** in partial fulfillment of the requirements for the degree of **Master of Science** i**n Civil Engineering, Middle East Technical University** by,

Prof. Dr. Halil Kalıpçılar
Dean, Graduate School of **Natural and Applied Sciences** _____

Prof. Dr. Erdem Canbay
Head of the Department, **Civil Engineering** _____

Asst. Prof. Dr. Cüneyt Baykal
Supervisor, **Civil Engineering, METU** _____

Examining Committee Members:

Prof. Dr. Ahmet Cevdet Yalçıner
Civil Engineering, METU _____

Asst. Prof. Dr. Cüneyt Baykal
Civil Engineering, METU _____

Prof. Dr. Mete Köken
Civil Engineering, METU _____

Asst. Prof. Dr. Gülizar Özyurt Tarakcıoğlu
Civil Engineering, METU _____

Assoc. Prof. Dr. Veysel Şadan Özgür Kırca
Civil Engineering, Istanbul Technical University _____

Date: 08.02.2022

I hereby declare that all information in this document has been obtained and presented in accordance with academic rules and ethical conduct. I also declare that, as required by these rules and conduct, I have fully cited and referenced all material and results that are not original to this work.

Name Last Name : Semih Batuhan Çandır

Signature :

ABSTRACT

INVESTIGATION OF NUMERICAL SCHEMES AND THEIR EFFECTS ON IMPACT PRESSURES IN NUMERICAL MODELLING

Çandır, Semih Batuhan
Master of Science, Civil Engineering
Supervisor : Asst. Prof. Dr. Cüneyt Baykal

February 2022, 77 pages

Impact pressure is generated with the high-speed fluid impact into a stationary solid or vice versa. Impact pressure is a phenomenon that has been studied extensively in ship hydrodynamics, but the exact determination of forces acting on a coastal structure in a numerical environment has been a challenge for coastal engineers for a long time. Due to their complex structure of a two-phase flow involving both water and air, it is very time-consuming to properly model and solve this type of problem. This study aims to investigate different numerical schemes and their effects on the impact pressures. A dam break case was used to determine the performance of these numerical schemes, and the numerical model was validated using a physical experiment. Percent error was used to compare the peak pressure value accuracies between schemes, and root mean square and mean absolute errors were used to assess the overall performance of the numerical model. This study might provide a basis for numerical modelling studies on numerical approaches depending on the aim of the research. It is possible to improve the peak pressure prediction performance up to 99% and overall performance up to 37.5% using specific scheme combinations.

Keywords: impact pressure, dam break, numerical model, numerical schemes

ÖZ

SAYISAL MODELLERDE SAYISAL ŞEMALAR VE ÇARPMA BASINCI ÜSTÜNDEKİ ETKİLERİNİN İNCELENMESİ

Çandır, Semih Batuhan
Yüksek Lisans, İnşaat Mühendisliği
Tez Yöneticisi: Dr. Öğretim Üyesi Cüneyt Baykal

Şubat 2022, 77 sayfa

Çarpma basıncı yüksek hızlı sıvının duran bir katıyla ani teması veya tam aksinin gerçekleşmesiyle oluşur. Çarpma, gemi hidromekaniğinde kapsamlı bir şekilde araştırılmış olmasına rağmen, kıyı yapılarına etki eden kuvvetlerin sayısal ortamda kesin sonuçlarının belirlenmesi kıyı mühendisleri için zorlayıcı olmuştur. Su ve havadan oluşan çift fazlı akışın karmaşık yapısı sebebiyle, problemlerin doğru bir şekilde modellenmesi ve çözülmesi bir hayli zaman almaktadır. Bu çalışmada, farklı sayısal şemalar ve bu şemaların çarpma basıncı üzerindeki etkilerinin incelenmesi amaçlanmıştır. Şema performanslarının belirlenmesi için bir baraj yıkılması örneği kullanılmış ve sayısal model fiziksel bir deney kullanılarak doğrulanmıştır. Şemalar arasında en yüksek basınç değerinin doğruluğu için yüzdesel hata kullanılırken, modellerin genel performans değerlendirmesinde ortalama karesel hata ve ortalama mutlak hata kullanılmıştır. Çalışmanın sayısal model çalışmalarında araştırmanın amacına uygun yaklaşımların belirlenmesinde temel oluşturması beklenmektedir. Belirli şema kombinasyonları kullanılarak en yüksek basınç tahmini performansının %99 oranında artırılması, bunun yanında sonuçlar genelinde %37.5'e varan iyileştirmeler sağlanmasının mümkün olduğu tespit edilmiştir.

Anahtar Kelimeler: çarpma basıncı, baraj yıkılması, sayısal model, sayısal şemalar

To my beloved family and parents

ACKNOWLEDGMENTS

I would like to express my deepest gratitude to my supervisor Asst. Prof. Dr. Cüneyt Baykal for guiding me, advising on how to improve the study, criticism, encouragements, and insight throughout the research.

I would also like to thank Hasan Gökhan Güler for his suggestions, comments, and endless help and encouragement throughout the study.

I would also like to express my special thanks to Umman Özlem Zeybek for all the complimentary support, advice, and unconditional love she offered. This study would not be completed if she was not always there for me.

Finally, I would also like to express my sincere gratitude to my mother, Tuğba Çandır, my father, Abdullah Çandır, and my brother, Berke Ozan Çandır for their support, belief, and encouragements throughout the challenging times. They were always there for me whenever I needed them.

TABLE OF CONTENTS

APPENDICES

LIST OF TABLES

TABLES

LIST OF FIGURES

FIGURES

LIST OF ABBREVIATIONS

ABBREVIATIONS

1-D	One-dimensional
2-D	Two-dimensional
3-D	Three-dimensional
CFD	Computational Fluid Dynamics
CFL	Courant-Friedrichs-Lewy
CICSAM	Compressive Interface Capturing Scheme for Arbitrary Meshes
CIP	Constrained Interpolation Profile
ELP	Elementary Loading Process
MARIN	Maritime Research Institute Netherlands
MPS	Moving Particle Semi-implicit
MULES	Multidimensional Universal Limiter with Explicit Solution
MUSCL	Monotonic upstream-centered scheme for conservation laws
NMAE	Normalized Mean Absolute Error
NRMSE	Normalized Root Mean Square Error
NVD	Normalized Variable Diagram
OpenFOAM	Open Source Field Operation and Manipulation
PE	Percent Error
PISO	Pressure-implicit Split-operator
QUICK	Quadratic Upstream Interpolation for Convective Kinematics

RANS	Reynolds Averaged Navier-Stokes
SFCD	Self-filtered Central Differencing
SIMPLE	Semi-implicit method for pressure-linked equations
THINC	Tangent of hyperbola for interface capturing
TVD	Total Variation Diminishing
UMIST	Upstream Monotonic Interpolation for Scalar Transport
VOF	Volume of Fluid

LIST OF SYMBOLS

SYMBOLS

α	VOF-indicator function
α_f	VOF-indicator function for cell face f
$\alpha_{f,upwind}$	Upwinded VOF-indicator function for cell face f
α_{rf}	Compressive VOF-indicator function for cell face f
Δx	Distance between cell faces along the x-direction
Δy	Distance between cell faces along the y-direction
λ_M	MULES delimiter
μ	Viscous dynamic viscosity
μ_g	Dynamic viscosity of the gas
μ_l	Dynamic viscosity of the liquid
μ_t	Turbulent dynamic viscosity
ρ	Density
ρ_g	Density of gas
ρ_l	Density of liquid
σ_{exp}	Standard deviation of the reference experimental data
ϕ	General variable
ϕ_f	Volume flux for cell face f
ϕ_{rf}	Compressive volume flux for cell face f

Ω_i	Volume corresponding to the ith element of the physical domain
Co	Courant-Friedrichs-Lewy Number
F_c	Interfacial compression flux
F_u	Upwind convective flux
g	Gravitational acceleration
N	Total number of data points
p	Pressure
t	Time
u	Velocity in the x-direction
u_i	Velocity in ith direction
u_i^g	Velocity of gas in ith direction
u_i^l	Velocity of liquid in ith direction
u_i^r	Compressive velocity in ith direction
v	Velocity in the y-direction
$\vec{V}$	Velocity vector
x_i	Coordinate in ith direction
y_{exp}	Value obtained in the reference experiment
$y_{i,exp}$	ith value of the reference experiment
$\overline{y_{exp}}$	Mean value of the reference experimental data
y_{model}	Value obtained in the numerical model
$y_{i,model}$	ith value of the numerical model

CHAPTER 1

INTRODUCTION

From the earliest stages of human life, coastal areas have been attractive places for people because they have two primary needs to survive: food and water. Building settlements around coastal areas arose other needs as a result, which are access and protection. Coastal structures like harbors and breakwaters are built to reach overseas or protect the coast. With the growing technology, people even started to build structures on the seas. These improvements resulted in a challenge for people to solve. Coastal structures should endure against the wave-induced forces. It is essential to start from the interactions between the wave and the structure to understand these forces. That is why solid-fluid interaction is a great concern for coastal and ocean engineering.

Generally, small-scale models of coastal structures are used to determine the wave-induced forces acting on the structure. Several types of waves, including wind-generated, tidal waves and tsunamis, can be modeled to study this interaction between solid and fluid. Breaking waves of any type are the most violent due to the amount of energy released. Thus, modelling breaking waves is one of the major coastal and ocean engineering problems. The high energy release results in huge pressures applied on structures, and the impact pressure is one of those. Similarly, waves are formed during the dam break event, where a massive fluid body is released instantly. The waves formed after the event are also breaking on the structures, resulting in impact pressures as well.

Inevitably, the physical modelling stage is very time-consuming, and repeating the experiments is relatively challenging. With the invention of high-capacity computers, it became more and more convenient to model coastal problems in a numerical environment due to ease in repeating the test and relatively cheap

modelling stage. The physical conditions of the coastal problem are reproduced numerically, and the relation between solid and fluid is examined by solving governing equations. Numerical schemes are utilized to discretize these governing equations. A numerical solution algorithm is then applied to discretized equations to make predictions regarding the velocity and pressure fields along the computational domains. There are numerous numerical studies on the wave-structure interaction, including impact pressures. Despite the wide range of studies within this field, there is no general study concerning the effect of the numerical schemes on the prediction of pressure, and specifically, impact pressures.

This study aims to investigate different numerical schemes and their effects on the computation of impact pressure caused by the violent impact of the fluid on structures. Results obtained with different schemes are evaluated depending on a reference physical experiment to assess the performance of the schemes. This reference experimental case is a dam break problem, which is selected in this study due to its convenience to carry out simulations investigating the effect of the numerical schemes in predicting the impact pressures. The dam break problems can be studied in relatively small regions, and the representative duration of these events is much shorter compared to studies focusing on wind-generated waves in both experimental and numerical studies.

In Chapter 2, literature is summarized in two main parts. First, an overview of the dam break phenomenon and impact pressure is given, and then, studies on physical and numerical modelling of dam break phenomenon are presented.

In Chapter 3, information on numerical modelling is given in detail, starting from the reference physical model experiment, including the experimental setup, physical properties of the fluid and data acquisition methods. Then, details of the numerical model used to investigate the numerical schemes are presented. The investigations are carried out using a numerical solver, interFoam, based on the OpenFOAM, a computational fluid dynamics (CFD) Library. An overview of the numerical environment is given in this chapter. Reynolds Averaged Navier Stokes (RANS)

equations are solved in interFoam, and the details are presented in this chapter. interFoam uses the volume of fluid (VOF) method to capture free surface; details of the method are also given in this chapter. Numerical solution algorithms and investigated numerical schemes are presented in the latter part of this chapter. Then, the computational mesh used to reproduce the experimental setup and corresponding boundary conditions are also given in this chapter. Finally, simulations and the investigation methodology are presented here.

In Chapter 4, the simulation results are given for each investigation. The performances of the simulations are evaluated and compared using error analysis. Percent error (PE), normalized root mean square error (NRMSE) and normalized mean absolute error (NMAE) are used in the error analysis.

In Chapter 5, a summary of the present study is given, and the conclusions of the investigation are presented. The recommendations for future work are also expressed here.

CHAPTER 2

LITERATURE REVIEW

Solid-fluid interactions have been studied for a long time, yet there is no holistic answer to some of the questions in computational fluid dynamics (CFD). Breaking waves and their violent impact on the coastal structures is one of them, where there are plenty of open questions. Phase interactions between solid and fluid phases and their impacts are studied both physically and numerically, and there are some difficulties in both. As it is a real challenge to observe and measure impact pressures with high accuracy in physical experiments mainly due to the sensitivity of the experimental equipment, it is also hard to reproduce the phase interactions correctly for the numerical experiments as a result of rapid change in velocity gradients. Despite the difficulties, dam break cases are widely studied by coastal engineers as these involve similarities to the coastal dynamics problems. Generally, a tank with two separate sections divided by a plate is used to experiment dam break cases. A similar setup is produced for numerical simulations using CFD tools, as shown in Figure 2.1. There are several options to choose from a wide range of CFD software in the numerical environment. In this study, OpenFOAM CFD Library is used for numerical analysis due to:

- Its readily available linear solvers, numerical schemes and solution algorithms.
- Its increasing usage in coastal and ocean engineering applications
- Its open-source library allows users to create, modify and use

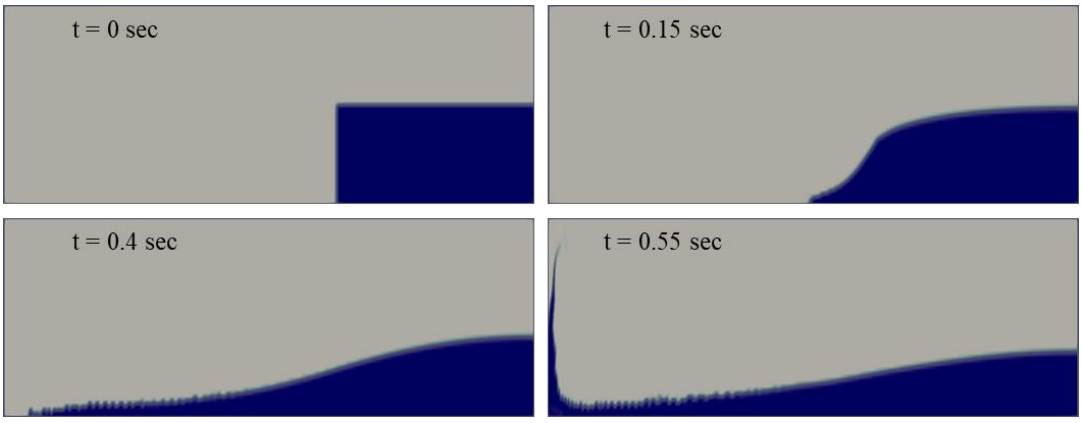

Figure 2.1. Dam break case stages

2.1 Overview of dam break phenomenon and impact pressure

One of the easiest ways to reproduce the violent nature of fluids on solid structures is the dam break cases. Dam break case studies date back to the 19th century, as Lobovský et al. (2014) mentioned in their experimental study conducted at the Technical University of Madrid. Even though numerous experimental studies are conducted on dam break cases, its dynamics are still not very well described. Mokrani & Abadie (2016) points out the natural occurrence of dam break as solid-fluid interaction occurs first, and it is followed by a relatively stationary stage. A dam break case is studied using a large volume of fluid. After releasing the fluid body, it moves towards a stationary obstacle or directly to the vertical wall. When the water body reaches the stationary object, huge pressure is applied on the structure due to the rapid expansion of the contact region between the solid and fluid, as Dias & Ghidaglia (2018) explained. This pressure is not the only force involved in this phenomenon. Lafeber et al. (2012) introduced Elementary Loading Processes (ELP) to further describe the involving loads on the vertical body. There are three types of ELP which are ELP1, ELP2 and ELP3. ELP1 is the direct impact, ELP2 is the building jet along the structure, and ELP3 describes the compression effect of the entrapped gasses. A representative image of these three types of ELP at different time instances is given in Figure 2.2. There could be different combinations of these

three types of ELPs involved in the dam break cases. ELP1, the direct impact loads occur where the velocity component normal to the wall falls to zero rapidly, and a hemispherical pressure arises causing a hemispherical strain into the vertical wall. Peregrine (2003) explains the impact pressure as the timescale in which the peak pressure involved is too short for times of approximately 1 millisecond in laboratory conditions corresponding to 10 to 100 milliseconds in the field, and a sharp movement is observed in the pressure-time history.

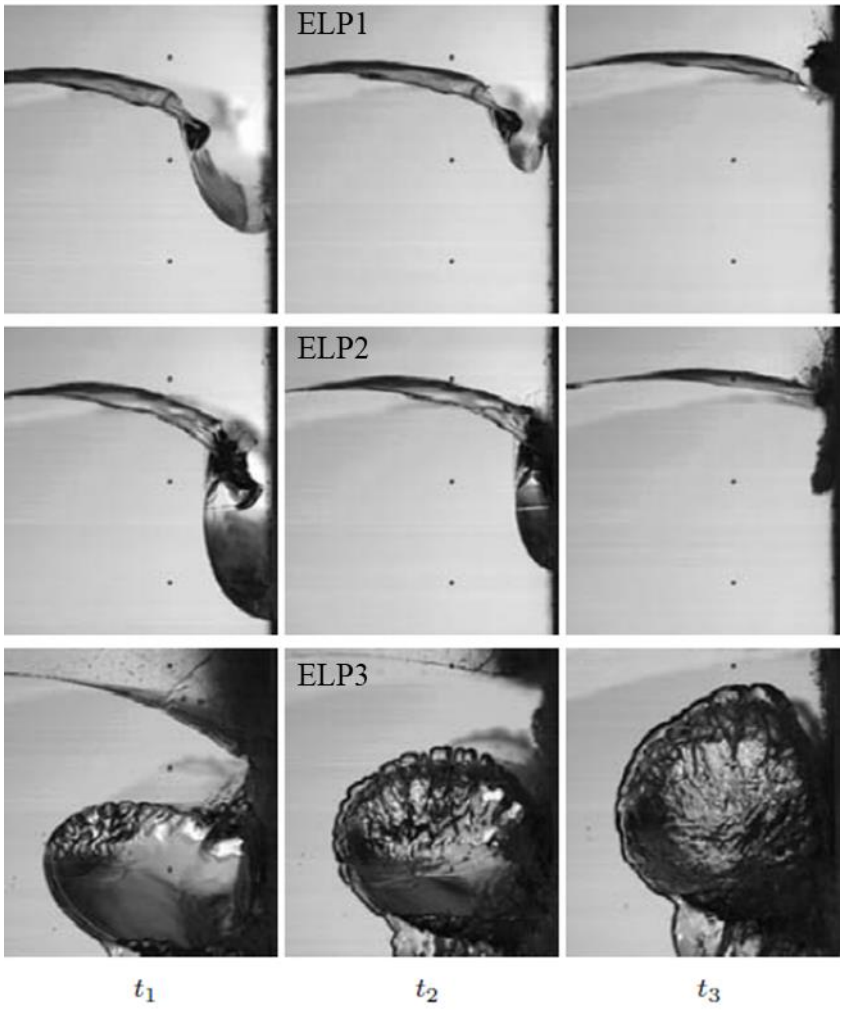

Figure 2.2. Representative image of ELP types (adopted from Lafeber et al., 2012)

Oumeraci et al. (2001) made a similar description of the impact loads where they studied new methods to calculate forces under severe impact conditions.

Identification of loads induced by waves is based on the behavior of pressure-time history, as shown in Figure 2.3. In Figure 2.3, F_h represents the horizontal force applied, while t/T is the dimensionless time where t is the duration and T is the wave period. They also indicate that although the impact pressure is an important parameter to assess solid-fluid interaction and structural response under impact loads, the duration of the impact pressure on the structure is also a great concern.

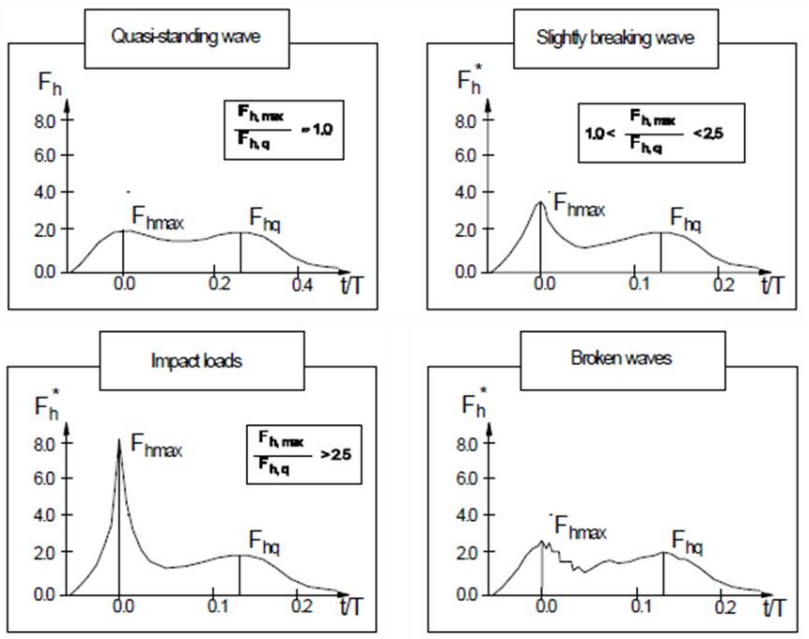

Figure 2.3. Identification of wave loads (adopted from Oumeraci et al., 2001)

Similar to Oumeraci et al. (2001), Lobovský et al. (2014) suggest the rise and decay time of the event can be calculated using a triangular approach theory, and the impact duration can be determined. The maximum pressure value observed is taken as a pivot point to determine the impact duration, and the duration Δt which the pressure value rises from half-maximal to the maximum point on the pressure-time history is calculated, twice this duration is described as the rise time. A similar procedure is applied for the decay time. The duration $\Delta t'$ where the pressure value drops from maximum value to half-maximal value is determined, twice this duration is described as decay time. The summation of the rise and decay time is considered as the impact duration, as shown in Figure 2.4.

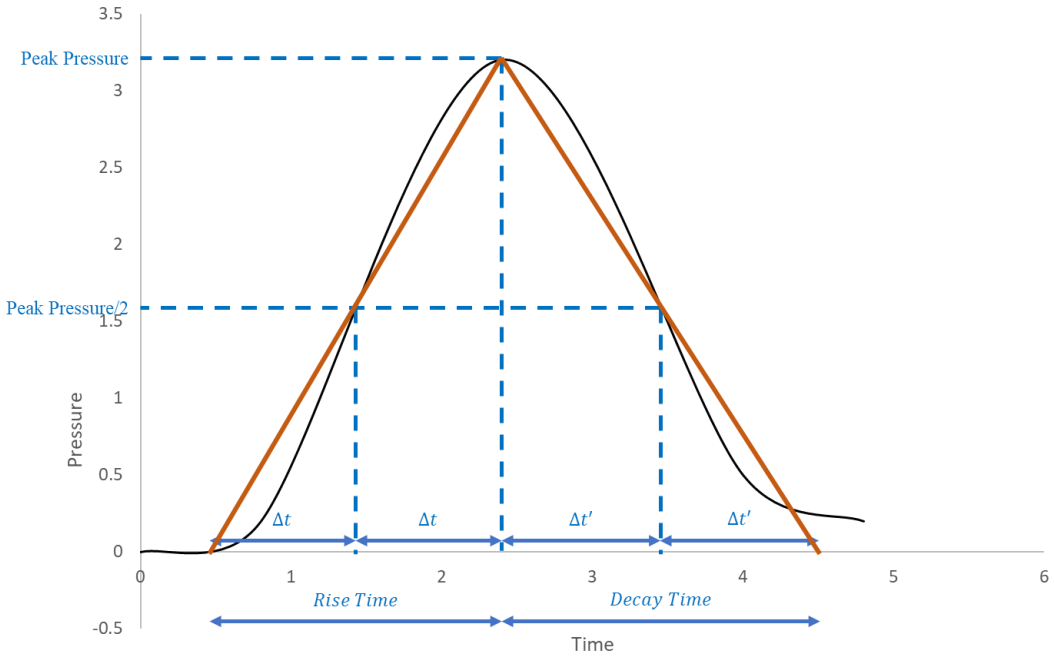

Figure 2.4. Rise & decay time definition (adapted from Lobovský et al., 2014)

2.2 Physical and numerical modelling of dam break phenomenon

As discussed in the previous section, dam break cases are widely used in assessing impact pressures. There are several novel studies including a dam break case considering the different stages of the flow and the different aspects of the fluid motion.

Stansby et al. (1998) have studied the initial stages of the dam break flow at two different scales in a horizontal flume 15.24 by 0.4 meters, and the flume was separated with a vertical plate. Two sides of the flume are filled with different water levels, and the plate is instantly removed. Experimental results are compared with the solutions obtained using shallow-water equations, and the results are in good agreement with the equations except just after the release where jet-like formations are observed, and the interactions are rather complex to be computed fully accurate.

Zhou et al. (1999) and Lee et al. (2002) have used an experimental setup studied at the Maritime Research Institute Netherlands (MARIN) to validate their numerical solutions. This setup consists of a 3.22-meter-long wave tank with a width of 1 meter. The tank is divided into two parts with a vertical flap, one of which is a dry bed, and the other one is filled with water. Three different pressure transducers are placed at the end of the tank, and impact pressures applied on the transducers are measured.

Zhou et al. (1999) aimed to predict the three-dimensional flow model of green water loading on and off the deck of the ship and their impact pressures on the structural body. The experimental setup is used to validate the proposed numerical model.

Lee et al. (2002) also used this experimental setup to validate their numerical approach on water sloshing and water impacting. Glimm's method is applied to the numerical investigation of hydraulic jumps that occurred during the sloshing motion. Spatial and temporal discretization effects are examined. Readers are referred to Glimm (1965) for further detail on Glimm's method.

Bukreev et al. (2004) have prepared an experimental setup to determine complex channel geometry and frictional energy loss effects on the dam break cases. To thoroughly analyze the processes, they have used both dry and flooded bottom scenarios in their experiments. 3.3 by 1.00 m reservoir tank is filled with water, and a vertical flat gate is used to separate the end of the channel from the reservoir tank. Dry bottom and flooded bottom cases with an initial water height before the gate removal are generated using the experimental setup. Experimental results are then used to verify the theoretical approach proposed.

Hu & Kashiwagi (2004) explain why the dam break case is used in numerical models so often as implementing the initial and boundary conditions for the dam break case is simple. In their numerical study, the aim was to determine if the implemented method is capable of predicting the wave-body interactions correctly. They used a dam break experiment conducted in the Research Institute for Applied Mechanics, Kyushu University, to validate their work using a single circular pressure sensor at the end of the tank.

Kleefsman et al. (2005) proposed a calculation method for wave impact problems using Navier-Stokes equations for incompressible viscous flows. Experiments performed at MARIN for breaking dam case is used to validate the proposed prediction method. Tank dimensions are the same as the previous MARIN experiments, but a stationary obstacle is placed in the dry bottom area, and eight different pressure transducers are used to determine the applied pressure loads on the structure. They have used their experimental setup to validate their calculation method. In their study, compared pressure time histories show several spikes occurring in the prediction method and this occurrence is explained as the conversion of an empty cell to a fully wetted cell during one time step. Other than these spikes, simulations show good agreement with the experimental data. However, in the present study, it is seen that it is possible to prevent the generation of these spikes by applying appropriate numerical schemes to the solution method.

Bukreev & Gusev (2005) have also studied the initial stages of the dam break case. They have investigated both shallow-water equations and Navier-Stokes equations in their studies to describe the initial stages of the dam break. They have concluded the study as neither of these approaches is enough to describe the real processes.

Wemmenhove et al. (2010) have studied sloshing motion focused on a single impact, and they investigated the interaction between the fluid and the structure using two different simulation programs. They have used the dam break experiment as their validation method to numerical models using an experimental setup conducted at MARIN with the same dimensions as the previous MARIN experiments. Seven pressure transducers are used to investigate the fluid impact on the vertical wall located at the end of the dry bottom part. Effects of the wall flexibility are also included in this study, and the difference between rigid and flexible wall is observed.

Hu & Sueyoshi (2010) have prepared an experimental setup to introduce their numerical methods, namely Constrained Interpolation Profile (CIP) based Cartesian grid method and the Moving Particle Semi-implicit (MPS) method. They have used a rectangular tank with the dimensions of 80 by 20 cm separated with a partition

plate to experiment the dam break case to compare these two methods developed and improved by the authors. In their study, they have investigated water front speed using these two methods and compared their results with their experimental setups. Introduced methods showed a good agreement with the experimental results considering the water front speed. On the other hand, water front speed is not enough to assess the complex motion of fluid flow and the solid-fluid interactions, as shown in their comparison figures.

Ji et al. (2013) further examined the case by considering an incompressible flow but validating their results with the same small-scale experiment and previously mentioned larger scale experiment, MARIN experimental setup, both having a single pressure point at the end of the tank. They have studied the case to determine the performance of a CIP-based model using the tangent of hyperbola for interface capturing (THINC) scheme. Even though small-scale experiment shows an acceptable agreement with the numerical results overall, impact pressures are overpredicted. For the large-scale experiment, numerical results fail to show the impact pressures accurately, although the quasi-static stage is in good agreement with the experimental data.

Lobovský et al. (2014) prepared a similar setup to MARIN scaled 2:1 at the Technical University of Madrid, and they aimed to measure impact pressures on the vertical wall at the end of the tank and vertical propagation of the pressure along the wall. They have placed four pressure sensors starting from the very bottom of the tank at the centerline to achieve this. Another sensor is placed halfway towards the back wall to discuss the three-dimensional (3-D) effects that may occur in the wave loads.

Marsooli & Wu (2014) have studied the dam break case using the Volume of Fluid (VOF) method combined with Compressive Interface Capturing Scheme for Arbitrary Meshes (CICSAM) solving the Reynolds Averaged Navier-Stokes (RANS) equations. The 3-D features of the flow at the initial stage of dam break were examined and compared with the experimental data. Results show a good

agreement regarding the trend of the pressure-time history, but impact pressures at the solid-fluid interaction are overpredicted with the used method.

Das & Bagheri (2015) have studied the dam break case using MacCormack-type schemes in their numerical methods. They used second and fourth-order MacCormack schemes to solve shallow-water equations and compared their results with the experimental data. Numerical schemes were applied to both one-dimensional (1-D) and two-dimensional (2-D) cases for both dry and wet bed conditions. Water levels and velocities were compared with the experimental data for all the cases, but there was no information about the impact pressures.

Zhang et al. (2017) have studied the dam break case using a 3-D unstructured mesh finite element model with Navier-Stokes equations. They have used an L-shaped channel to simulate the dam break case, and the results were compared with the experimental data. Velocity vectors in the reservoir and streamlines on the channel were also examined, and the free surface levels obtained from the numerical model were compared. A general trend in the water flow characteristics was obtained with minor discrepancies, but the impact pressures applied on the elbow are not investigated in this study.

Chen et al. (2019) have studied the 3-D numerical model of green water loading on deck using a dam break model. VOF method is applied to the model solving Navier-Stokes equations by OpenFOAM. A great computational effort is needed for the solution of the numerical model since they have tried to make a similar model as much as possible to the experimental model used to validate the numerical results. A good agreement was ensured in the pressure-time history of the numerical results with experimental data. However, the first peak is overpredicted, and the second peak is underpredicted with the used methodology.

Güler (2020) have studied a numerical model to establish a CFD solver based on immersed boundary method. CFD solver ibmPorFoam developed by the author is validated using two different dam break cases, one of which is previously mentioned Kleefsman et al. (2005). During the validation process, the performance of different

interpolation schemes is studied considering the velocity parameter of the convective term, which creates the basis of this study. Despite the promising results obtained through the study, further improvements may be added by removing the parameter limitations with a detailed investigation.

Peng et al. (2021) have studied a RANS equation-based numerical model to discuss the interaction of the dam break flood with a structure. The aim was to clarify the dam break flood effects on the structure and the influence of the initial water level on the impact pressure. In order to validate their results, an experimental setup installed at the Technical University of Madrid is used. The numerical simulation results fall in the confidence range of the experimental data, but the evolution of the impact pressure is lagged due to turbulent flow characteristics.

CHAPTER 3

NUMERICAL MODELLING

A numerical modelling study is performed in the OpenFOAM environment to investigate the effects of different numerical schemes on impact pressure prediction. The prediction performance of the numerical schemes is examined using this numerical model. Pressure-time histories obtained from a physical experiment are used as a reference to assess the performance of different models. Each simulation run is evaluated based on the performance of the peak pressure value determination and the performance of the overall pressure value determination.

Information about the reference experimental study that was used to assess the performance of the numerical model, detailed information on the experimental setup, physical properties of the test fluid and data acquisition techniques are given in this chapter.

This chapter will also include the overview of the numerical model, governing equations, surface capturing method, numerical schemes and numerical solution algorithms, properties of the computational mesh and boundary conditions for the numerical model.

The simulations prepared for investigation and the corresponding methodology behind them are given in this chapter.

3.1 Reference Physical Model Experiment

The experimental setup used as a reference case in this study was performed by Lobovský et al. (2014) at the Technical University of Madrid. The reason for selecting this study as the reference case is that the experiment was designed to serve for CFD analysis, and special attention has been given to the impact pressure

measurements, which is the main focus of this numerical study. Sample data, statistical analysis, figures and video recordings are publicly available. Experiments for two different initial water heights (i.e., the height of the dams), which are 300 mm and 600 mm, were performed, and the experiments were repeated 100 times. Details of the experimental setup will be given in the following sections.

3.1.1 Experimental Setup

As Lobovský et al. (2014) described, a dedicated prismatic tank was designed and built consisting of two separate parts divided by a vertical plate with a sliding mechanism. One part is filled with water to a specific level, and the other is the dry bed. A weight was attached to the vertical plate to simulate dam break motion. A schematic view of the experimental setup is given in Figure 3.1. Experiment with 300 mm water height is used as the reference case in this study.

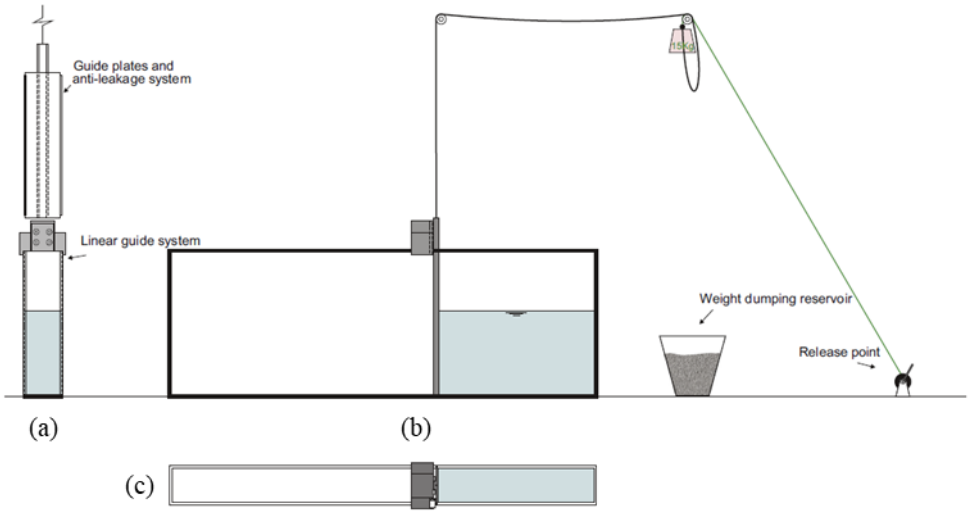

Figure 3.1. Schematic view of the experimental setup (adopted from Lobovský et al., 2014) (a). side view (b). front view (c). plan view

The prismatic tank used in the experiments has a length of 1610 mm and a width of 150 mm. Water levels inside the prismatic tank were measured at four different locations along the x-axis, five different pressure transducers were placed at the left

end of the prismatic tank to determine the pressure-time history during the experiment. Dimensions of the prismatic tank and data acquisition locations are given in Figure 3.2.

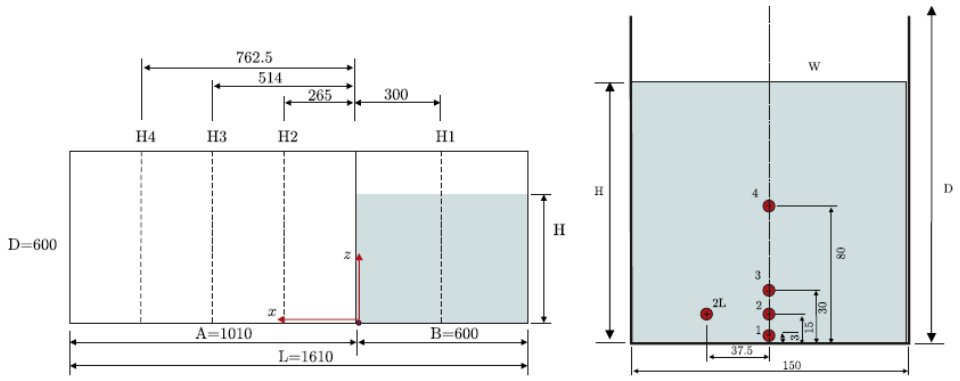

Figure 3.2. Dimensions of the tank & data acquisition locations (adopted from Lobovský et al., 2014)

3.1.2 Physical Properties

Lobovský et al. (2014) have used fresh water in their experiments, the temperature of the water was controlled with an error margin of ± 0.1 °C, and it was preheated to 25 °C before each experimental run. Under these conditions, fresh water used in the experiment was considered a Newtonian fluid with a density of 997 kg/m^3, the kinematic viscosity of 8.9 × 10^{-7} m^2/s, and surface tension of 0.072 N/m. In order to record digital images and videos of the experiment, the fluid was dyed with fluorescein in some of the runs. No significant influence was observed on the fluid dynamics with the dyed fluid in the experiments.

The gate of the dam was made of 10 mm thick polymethyl methacrylate and placed into side rails to keep the movement unobstructed. 15 kg of weight was connected to the plate using a steel wire and placed upon a weight dumping reservoir. The theoretical velocity of the weight is calculated as 4.65 m/s.

3.1.3 Data Acquisition

Lobovský et al. (2014) have used five different pressure sensors to obtain impact pressure values at the end of the dry bottom part. Sensor-1 was placed at the tank bottom, which means the center of the sensor is located 3 mm above the horizontal bed. Sensor-2 was placed 15 mm above the bed to compare the experimental results with Wemmenhove et al. (2010). Sensor-3 was placed 30 mm above the bed as Kleefsman et al. (2005) have used in their experiments, and Sensor-4 was placed 80 mm above the bed as Lee et al. (2002) have used in their experiments. Sensor-2L was placed off-centered to determine the 3-D effects of the flow on the impact pressure. Sensor locations are given in Figure 3.2. Sensors used in the experiment have a sensing diameter of 4.2 mm around their center, and the signals were recorded with a sampling rate of 20 kHz. Recorded videos have been used to obtain water levels through the tank. The digital camera used to capture video records is capable of recording 300 frames per second at a resolution of 512 by 384 pixels. Water level measurement locations are given in Figure 3.2. The data obtained from the experiment is non-dimensionalized to represent the behavior of the system independent from the dimensions. The pressure and time parameters are non-dimensionalized using $\rho g H$ and $\sqrt{H/g}$, respectively.

3.2 Numerical Model

The numerical modelling study is performed based on the information given in the reference experimental setup, assuming a viscous and incompressible fluid flow.

3.2.1 Overview of OpenFOAM Environment

As OpenFOAM User Guide (2019) describes, Open Source Field Operation and Manipulation (OpenFOAM) is a C++ library that offers the ability to create solvers designed to solve a specific problem or utilities designed to perform tasks on data

manipulation. Besides that, it is possible to pre- or post-process the data with OpenFOAM, which makes data handling more consistent.

Pre-processing tools allow users to generate different types of meshes or load a generated computational mesh into the system. On the other hand, post-processing tools provide users with visualization of the model in various displaying options.

Each solver in OpenFOAM CFD Library has a unique structure where continuity and momentum conservation equations are solved simultaneously. The generic conservation equation in OpenFOAM is given in Equation 3.1,

$$\frac{\partial \rho U}{\partial t} + \nabla \cdot \phi U = \nabla \cdot \mu \nabla U - \nabla p \qquad \text{Equation 3.1}$$

Several categories of numerical schemes are used to determine these terms in the generic conservation equation. As mentioned in OpenFOAM User Guide (2019), these categories can be specified as interpolation schemes, surface normal gradient schemes, gradient schemes, Laplacian schemes, divergence schemes and time schemes.

Time schemes are used to discretize the first term in Equation 3.1, and among time schemes, there are three prominent options: i) backward scheme, ii) Crank-Nicolson scheme, and iii) implicit Euler scheme. Moukalled et al. (2016) describe these time schemes in their book as implicit Euler scheme uses forward differencing while backward scheme uses backward differencing as the name implies. The Crank-Nicolson scheme can be considered as a combination of both. First, backward differencing is used implicitly and then forward differencing is applied explicitly.

Laplacian schemes are used to determine the diffusive term of the conservation equation, which corresponds to the third term in Equation 3.1. As described in the OpenFOAM User Guide (2019), the Gauss scheme is the only option for discretizing the diffusive term, while an interpolation scheme and surface normal gradient scheme should also be selected.

Interpolation schemes are selected from a vast number of options for each parameter of the convective term, which corresponds to the second term in Equation 3.1. However, for all parameters involved in the generic conservation equation, there should be a default interpolation scheme to interpolate the cell center values to the faces of the cell. For the present purpose, linear, midpoint and cubic schemes are available in the library.

Surface normal gradient schemes mentioned above are divided into five groups: corrected, uncorrected, limited, face corrected and orthogonal. The limited option uses a coefficient between 0 and 1 to apply a non-orthogonal correction. If the coefficient value is set to one, then the explicit non-orthogonal correction is applied, and if the value is set to zero, no non-orthogonal correction is applied. The face corrected option includes the non-orthogonal correction applied to the faces, and the orthogonal option applies correction, but non-orthogonality is ignored.

Gradient schemes are used on the gradients, corresponding to the fourth term in Equation 3.1. An optional limiter may also be used with gradient schemes. There are two options for the gradient schemes: i) Gauss and ii) least-squares schemes. The least-squares option applies the second-order least-squares scheme, while the fourth-order least-squares scheme can be applied with the fourth option. The scheme itself is sufficient for the least-squares option. On the other hand, an interpolation scheme should be specified for point-to-point interpolation if the Gauss scheme is used as the gradient scheme. Point-to-point interpolation here refers to the interpolation between cell center value to the faces of the cells. Cell limited or face limited optional limiter may also be specified to limit the extrapolated face values to a neighboring cell or face.

Finally, divergence schemes are used to determine the convective term in the generic conservation equation, which corresponds to the second term in Equation 3.1. Gauss scheme is the only option for the discretization here, and it requires an interpolation scheme besides that. Some of the numerical schemes used for point-to-point interpolation include but not limited to centered schemes, upwinded convection

schemes, Normalized Variable Diagram (NVD) and Total Variation Diminishing (TVD) schemes.

Further details and information on the numerical schemes used in this study will be given in the following sections.

3.2.2 Governing Equations

In this study, numerical modelling is carried out using a computational fluid dynamics (CFD) solver interFoam, a widely used tool in dam break modelling and developed based on the CFD library OpenFOAM. interFoam solves Reynolds Averaged Navier Stokes (RANS) equations to model the two-phase incompressible flow of water and air. The continuity equation in Equation 3.2 and the momentum equation in Equation 3.3 are simultaneously solved until the time limit specified for the numerical model is reached.

$$\frac{\partial u_i}{\partial x_i} = 0 \qquad \text{Equation 3.2}$$

$$\frac{\partial(\rho u_i)}{\partial t} + \frac{\partial(\rho u_i u_j)}{\partial x_j} = -\frac{\partial p}{\partial x_i} + \frac{\partial}{\partial x_j}\left[(\mu + \mu_t)\left(\frac{\partial u_i}{\partial x_j} + \frac{\partial u_j}{\partial x_i}\right)\right] + \rho g_i \qquad \text{Equation 3.3}$$

In Equation 3.2 and Equation 3.3, x_i is the coordinate, u_i is the corresponding velocity, ρ is the density, t is the time, p is the pressure, g_i is the gravitational acceleration, μ is the viscous dynamic viscosity and μ_t is the turbulent dynamic viscosity.

The convection term in the integral generic conservation equation can be expressed as in Equation 3.4, which corresponds to the second term in Equation 3.3,

$$\int_{CS} \rho\phi\vec{V} \cdot dA \qquad \text{Equation 3.4}$$

In Equation 3.3, ρ is the density, $\vec{V}$ is the velocity vector and ϕ is the general variable depending on the conservation type, and the equation represents the net flux of ϕ due to convection across the control surface out of the control volume. This convection term can be discretized for a cell in a 2-D cartesian grid as shown in Figure 3.3 using Equation 3.5.

$$\int_{CS} \rho\phi\vec{V} \cdot dA = \sum_{enws} \rho\phi u\Delta y - \sum_{enws} \rho\phi v\Delta x \qquad \text{Equation 3.5}$$

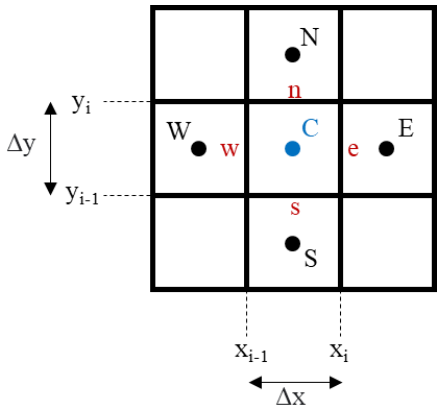

Figure 3.3. 2-D Cartesian grid & cell locations

In Equation 3.5, u is the velocity in x-direction, v is the velocity in the y-direction, Δx is the distance between cell faces along the x-direction, and Δy is the distance between cell faces along the y-direction. The term "enws" represents the east, north, west, and south faces of the cell denoted as C. Numerical schemes to find the values at the faces of the cell are called discretization schemes, and these are specific to each parameter involved in the conservation equation.

3.2.3 Turbulence Closure

Güler (2020) indicated that turbulence modelling with RANS equations tends to over-estimate turbulence beneath the dam break waves so that the pressure values obtained at the pressure transducer locations are lagged and do not represent the

experimental results. Besides that, Lobovský et al. (2014) define the flow as laminar in their experiment, based on the observations at the initial stages of the dam break event. Thus, turbulence modelling is excluded in this study to better represent the experimental environment and turbulent dynamic viscosity μ_t is equal to 0 in Equation 3.3.

3.2.4 Surface Capturing Method

The volume of fluid (VOF) method is used for surface capturing in interFoam solver. As indicated by Hirt & Nichols (1981), the VOF method offers a region-following scheme instead of a surface so that the method has fewer storage requirements. Therefore, the computational time is significantly reduced using this method. In the VOF method, the VOF-indicator function (α) is defined as the value of the function is equal to one for the cells fully occupied with fluid, and the value is equal to zero if there is no fluid inside the cell. Thus, the cell must contain a free surface for the values in between these. The VOF-advection equation in Equation 3.6 is solved to determine the free surface using the Multidimensional Universal Limiter with Explicit Solution (MULES) algorithm, limiting the indicator function value, α between 0 and 1.

$$\frac{\partial \alpha}{\partial t} + \frac{\partial \alpha u_i}{\partial x_i} + \frac{\partial \alpha(1-\alpha)u_i^r}{\partial x_i} = 0 \qquad \text{Equation 3.6}$$

In Equation 3.6, compression velocity, u_i^r is defined as in Equation 3.7. As Berberović et al. (2009) described in their study, compression here refers to the compression of the free surface into a sharper one and should not be confused with the compressible flow.

$$u_i^r = u_i^l - u_i^g \qquad \text{Equation 3.7}$$

In Equation 3.7, u_i^l is the velocity of the liquid phase and u_i^g is the velocity of the gas phase.

Density and kinematic viscosity are calculated using Equation 3.8 and Equation 3.9, respectively, for each cell depending on the VOF-indicator function value. In these equations, ρ_l and μ_l corresponds to the liquid properties while ρ_g and μ_g corresponds to the gas properties. That means when the VOF-indicator function α is equal to 1, density and kinematic viscosity are dependent only on the liquid phase or vice versa. For the values in between, density and kinematic viscosity values are computed using the multiphase properties within the cell.

$$\rho = \alpha\rho_l + (1-\alpha)\rho_g \qquad \text{Equation 3.8}$$

$$\mu = \alpha\mu_l + (1-\alpha)\mu_g \qquad \text{Equation 3.9}$$

As Deshpande et al. (2012) describe, Equation 3.6 can be rewritten in integral form as in Equation 3.10 for the physical domain, Ω consisting of both liquid and gas phases.

$$\int_{\Omega_i} \frac{\partial \alpha}{\partial t} dV + \int_{\partial\Omega_i} \alpha\vec{V} \cdot ndS = 0 \qquad \text{Equation 3.10}$$

The discretized version of Equation 3.10 is given in Equation 3.11.

$$\frac{\alpha_i^{n+1} - \alpha_i^n}{\Delta t} = -\frac{1}{|\Omega_i|} \sum_{f \in \partial\Omega_i} (F_u + \lambda_M F_c)^n \qquad \text{Equation 3.11}$$

In Equation 3.11, the unsteady term is discretized using the forward Euler scheme while the convective term is the summation over the cell faces f of Ω_i. Convective fluxes F_u and F_c are expressed as in Equation 3.12 and Equation 3.13, respectively. λ_M is another limiter implemented in the MULES algorithm, and it is equal to one in the interface region and equal to zero anywhere else.

$$F_u = \phi_f \alpha_{f,upwind} \qquad \text{Equation 3.12}$$

$$F_c = \phi_f \alpha_f + \phi_{rf} \alpha_f (1 - \alpha_f) - F_u \qquad \text{Equation 3.13}$$

When $\lambda_M = 0$, which corresponds to the fully liquid phase, the convective term is solved using the upwind scheme straightly. On the other hand, for the interface where $\lambda_M = 1$, this corresponds to a more complex solution combining the interfacial compression flux with upwind flux as in Equation 3.14.

$$F_u + \lambda_M F_c = \phi_f \alpha_f + \phi_{rf} \alpha_f (1 - \alpha_f) \qquad \text{Equation 3.14}$$

In interFoam, $\phi_f \alpha_f$ and $\phi_{rf} \alpha_f (1 - \alpha_f)$ terms are discretized using divergence schemes as in the integral generic conservation equation in Section 3.2.2.

3.2.5 Numerical Solution Algorithms

The numerical solution algorithm is the method used to predict the values of the parameters for each time instance. Direct and iterative methods can be used in this prediction. As Moukalled et al. (2016) describe, since an accurate solution is not needed at each iteration, direct methods are rarely used in CFD applications. Iterative methods are more appealing for CFD problems. In iterative methods, linear solvers are used to predict the values of each parameter. Linear solvers are supported by preconditioners and smoothers depending on the solver type.

As explained in OpenFOAM User Guide (2019), linear solver control is determined for each parameter first, and then, the solution under relaxation can be specified. Velocity and pressure solutions are iterative procedures using pressure-implicit split-operator (PISO) and semi-implicit method for pressure-linked equations (SIMPLE) algorithms.

The SIMPLE algorithm solves the momentum equation for pressure neglecting the velocity field. Discarding this term does not affect the final solution because it converges to zero at the end, as described in Moukalled et al. (2016). Since there is a missing term in the algorithm, the pressure equation is under-relaxed to achieve stability. A summary of the SIMPLE algorithm is given in Ferziger et al. (2020). Velocity and pressure values are estimated using the previously calculated values,

equations for the velocity components are solved, the pressure correction equation is solved, pressure and velocity values are corrected, and the process advances to the next iteration time if the solution has converged.

In the PISO algorithm, the neglected velocity field term is accounted as a part of the correction procedure, as mentioned in Moukalled et al. (2016). In addition to the SIMPLE algorithm steps at the start, the momentum equation is solved explicitly using the latest values of pressure and velocity. Then, pressure and velocity values are updated, solving the second pressure correction equation and correction is done for the desired number of corrector steps. The process is repeated until convergence is obtained.

In OpenFOAM, the PIMPLE algorithm combining PISO and SIMPLE algorithms is used for the solutions, as mentioned in OpenFOAM User Guide (2019). It allows using Courant-Friedrichs-Lewy (CFL) numbers greater than 1, combining these two algorithms together. The PIMPLE algorithm can also work in PISO mode, simply defining the number of outer correctors to zero. Holzmann (2016) describes the principle of the algorithm as a steady-state solution is obtained with under-relaxation at first, and then outer correction loops are performed until convergence is obtained explicitly. After the tolerance criterion is reached, the outer correction loop is terminated, and the process advances to the next time step.

3.2.6 Numerical Schemes

An introductory explanation of the numerical schemes is given in Section 3.2.1. As mentioned in previous sections, the study aims to investigate the numerical scheme performances on impact pressure prediction. Numerical schemes are used to predict the value of each parameter in the discretized conservation equation.

In this study, the Gauss scheme is selected for all schemes except for the time scheme which is chosen as the Euler scheme since this is the default option for the dam break case in this CFD Library. For the Laplacian schemes option, linear interpolation

scheme and corrected surface normal gradient scheme are selected as suggested in the dam break tutorial of the library. Recalling that, for all parameters involved in the generic conservation equation, there should be a default interpolation scheme to interpolate the cell center values to the faces of the cell. The default interpolation scheme is selected as the linear scheme, which is another suggested option in the dam break tutorial.

Using the Gauss scheme in the convective term of the discretized conservation equation requires an interpolation scheme option. Different interpolation scheme options are used to investigate their effect on the impact pressures obtained from the simulation, while other schemes are kept constant for a controlled performance test. The parameters involved in the convective term are as follows: velocity, volume flux and compression flux. Detailed information on these terms is given in Sections 3.2.2 and 3.2.4. The convective terms and their corresponding notation in OpenFOAM are tabulated in Table 3.1. From this point on, terms will be recalled with their notations in OpenFOAM.

Table 3.1. Convective terms and their corresponding notations in OpenFOAM

Term	**Notation in OpenFOAM**
$\rho\phi\vec{V}\cdot dA$	rhoPhi, U
$\phi_f\alpha_f$	phi, alpha
$\phi_{rf}\alpha_f(1-\alpha_f)$	phirb, alpha

Arikawa & Igorashi (2018) claimed that the impact pressure prediction in numerical modelling is highly dependent on the numerical interpolation schemes used for the convection term in the discretized conservation equations. Güler (2020) further studied the claim by performing a series of simulations using different schemes applied to the “rhoPhi, U” term in his thesis study.

In the present study, numerical interpolation schemes are studied in detail, both for “rhoPhi, U” and “phi, alpha” terms. Several different interpolation schemes,

including centering schemes, upwinded convection schemes, NVD and TVD schemes, are applied to the numerical model while all other parameters are kept constant. Interpolation schemes considered for the convective term are listed in Table 3.2.

Table 3.2. Numerical schemes list considered for convective term

#	**Numerical Scheme**	#	**Numerical Scheme**
01	linear	15	MUSCLV
02	midPoint	16	QUICK
03	upwind	17	QUICKV
04	linearUpwind	18	UMIST
05	limitedLinear, Coeff = 0.2	19	UMISTV
06	limitedLinear, Coeff = 0.4	20	vanAlbada
07	limitedLinear, Coeff = 0.6	21	vanAlbadaV
08	limitedLinear, Coeff = 0.8	22	SuperBee
09	limitedLinear, Coeff = 1.0	23	SuperBeeV
10	Minmod	24	SFCD
11	MinmodV	25	SFCDV
12	vanLeer	26	Gamma
13	vanLeerV	27	GammaV
14	MUSCL		

The detailed explanation of each interpolation scheme in Table 3.2 is given below.

Linear scheme is the central differencing method where the face value is directly interpolated between the owner cell and the neighbor. It is a widely used interpolation scheme, and most of the schemes are set to linear by default.

midPoint interpolation scheme is a centering scheme that is very similar to the linear interpolation scheme. The difference between these schemes is that while the linear scheme applies central differencing method for interpolation, midPoint scheme

weighs both owner and neighboring cells equally, resulting in an arithmetic mean between points independent of the distance between points to the cell face.

Spalding (1972) comparatively explains the upwind scheme using the central differencing method. The central difference method assumes the estimated values between grid points are linear, which causes the estimated solution to be equal to the exact solution only for the small values of the property. In contrast, with upwind differencing, estimations are performed between cells weighing the last grid point more, which implies, for example, a fluid crossing an interface possesses the property of the last grid cell which it passed, resulting in convergence for all values of the property.

OpenFOAM employs the linearUpwind scheme based on Warming & Beam (1976). In their study, the aim was to provide a hybrid scheme using the advantages of both McCormack and second-order upwind schemes. Replacing the corrector equation with an upwind corrector, they constructed a hybrid scheme that can be altered depending on the local necessary conditions.

limitedLinear scheme is a TVD scheme version where linear differencing is applied with a limiter function. Sweby's limiter function is used in this numerical scheme to stabilize the linear differencing. Readers are referred to Sweby (1984) for the details of the limiter function.

Minmod is another TVD scheme that uses a flux limiter to limit the derivatives to more realistic values. Roe (1986) initially proposed the Minmod scheme, and it is based on the second-order Lax-Wendroff scheme. The scheme switches between central differencing and linear upwind differencing when sharp gradients are observed and simply applies the first-order upwind scheme in the case of smooth gradients. As Waterson & Deconinck (2007) describes, the Minmod scheme is the lower bound of the TVD flux limiter diagram and one of the simplest methods to achieve bounded behavior.

van Leer (1974) describes the vanLeer interpolation scheme in his work, where he performed a series of research on finding the ultimate conservative difference scheme. In the first part of the series, the Lax-Wendroff scheme is made monotonic, but the process requires conservation form to be expensed. In order to provide a monotonic conservative scheme, the new scheme is based on Fromm's scheme. A comparison between the original Fromm's scheme, monotonic Fromm's scheme, which is the focus of the study and Godunov's scheme, is made within the study. The resulting approximation has a better performance than its original, costing only a 4/3 increase in the computational effort. Readers are referred to van Leer (1974) for further details on the vanLeer interpolation scheme.

Monotonic upstream-centered scheme for conservation laws (MUSCL) is described in the studies van Leer (1977) and van Leer (1979). The ultimate conservative difference scheme is aimed at continuing works, and the MUSCL scheme can be regarded as a sequel to Godunov's method. For a given order of consistency, the scheme can be made more accurate than the ordinary upstream-centered schemes. More detailed information about the MUSCL scheme can be found in van Leer (1977) and van Leer (1979).

Quadratic Upstream Interpolation for Convective Kinematics (QUICK) scheme is proposed by Leonard (1979). The aim was to construct a stable convective interpolation scheme with good accuracy. It is based on both central and upwind differencing schemes and since quadratic interpolation is used for the estimation, obtained truncation error is third-order which means highly accurate results can be obtained using the QUICK scheme.

Upstream Monotonic Interpolation for Scalar Transport (UMIST) scheme is a higher-order TVD scheme based on the QUICK scheme as it is described in Lien & Leschziner (1994). An alternative symmetric limiter is used in the UMIST scheme making the scheme a monotonic version of the QUICK scheme.

In their study, van Albada et al. (1982) proposed a TVD scheme based on the second-order upwind scheme. The aim of the study was to compare the numerical model

performances to solve astrophysical flow problems. The proposed scheme is compared with Beam, Godunov, McCormack schemes and flux-corrected transport methods. The performance of the proposed scheme is higher than the compared schemes, especially in coarser grid spaces.

SuperBee is the numerical scheme that appears to be the upper bound of the TVD flux limiter diagram, as Waterson & Deconinck (2007) state in their study. The scheme is very effective for the solutions with discontinuities, but its extensive use of first-order downwinding causes it to become over-compressive. Roe (1985) explains the SuperBee scheme in his work. After his first-order scheme work, Roe proposed a second-order monotonic scheme and inserted B-functions as subroutines to this scheme. A hypergeometric function is used so that the function is named Hyperbee, and B-function corresponding to the unswitched third-order scheme is named Superbee.

Self-filtered central differencing (SFCD) scheme is proposed by Ziman (1990), and it is based on Runchal's central differencing scheme, a non-conservative finite difference scheme. In SFCD, Runchal's method was adapted, making it a conservative bounded scheme. Whenever a turning point is encountered, the scheme sets the blending factor to zero and switches to upwind differencing to maintain boundedness. If the blending factor is set to unity, then the SFCD scheme reduces to linear upwind differencing, making the scheme a non-linear blend between upwind and linear upwind differencing schemes.

Jasak et al. (1999) studied a scheme that will produce a bounded, accurate and converged solution for unstructured meshes. Gamma scheme is an NVD scheme preserving the boundedness of the solution with the normalized variable approach. The Gamma scheme is based on the central differencing, and it is used wherever it satisfies the boundedness criterion. To guarantee boundedness, it also uses upwind differencing. Thus, there is a switching mechanism between these schemes.

In Table 3.2, schemes named MinmodV, vanLeerV etc., indicate the “V” version of the schemes where the limiter function is applied to the direction of the greatest change.

An example of the numerical scheme file in OpenFOAM is given in Figure 3.4.

```
/*--------------------------------*- C++ -*----------------------------------*\
| =========                 |                                                 |
| \\      /  F ield         | OpenFOAM: The Open Source CFD Toolbox           |
|  \\    /   O peration     | Version:  v1912                                 |
|   \\  /    A nd           | Website:  www.openfoam.com                      |
|    \\/     M anipulation  |                                                 |
\*---------------------------------------------------------------------------*/
FoamFile
{
    version     2.0;
    format      ascii;
    class       dictionary;
    location    "system";
    object      fvSchemes;
}
// * * * * * * * * * * * * * * * * * * * * * * * * * * * * * * * * * * * * * //

ddtSchemes
{
    default         Euler;
}

gradSchemes
{
    default         Gauss linear;
}

divSchemes
{
    div(rhoPhi,U)  Gauss linearUpwind grad(U);
    div(phi,alpha)  Gauss vanLeer;
    div(phirb,alpha) Gauss linear;
    div(((rho*nuEff)*dev2(T(grad(U))))) Gauss linear;
}

laplacianSchemes
{
    default         Gauss linear corrected;
}

interpolationSchemes
{
    default         linear;
}

snGradSchemes
{
    default         corrected;
}


// ************************************************************************* //
```

Figure 3.4. Example numerical scheme file, fvSchemes

3.2.7 Computational Mesh

Computational mesh in this study is separated into two versions, one of which is a 3-D computational mesh and the other one is 2-D. Dimensions of the 3-D computational mesh are given in Figure 3.5. The blue region in the figure indicates the fluid body at rest initially.

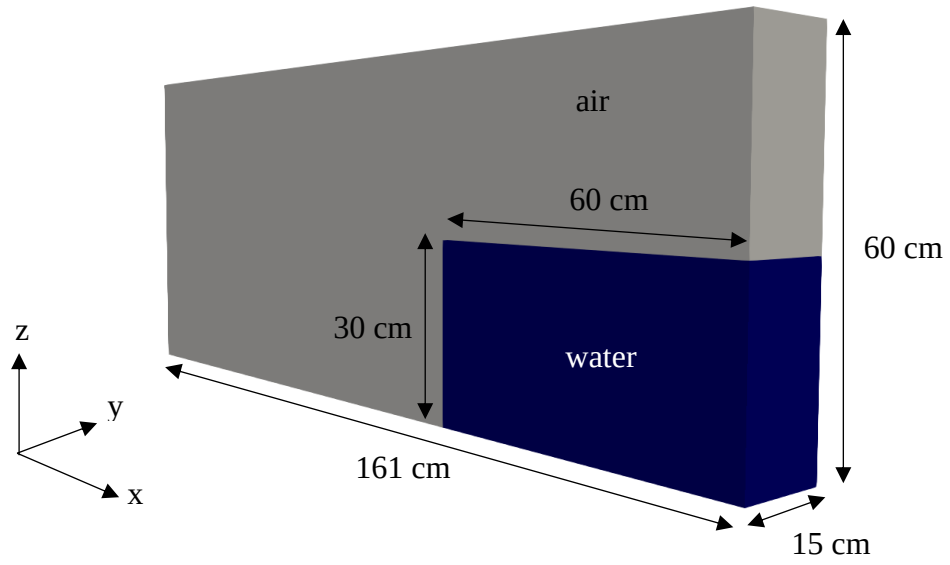

Figure 3.5. 3-D Computational mesh

In the 3-D computational mesh, the mesh size is constant in the y- and z-directions while a simple grading is applied in the x-direction which the ratio of the smallest mesh size to the greatest is 1:4. With this method, the computational time is decreased while the higher accuracy for impact pressure measurements is targeted with smaller mesh sizes at the point of interest. A representative image of the mesh sizes along the x- and y-directions are given in Figure 3.6.

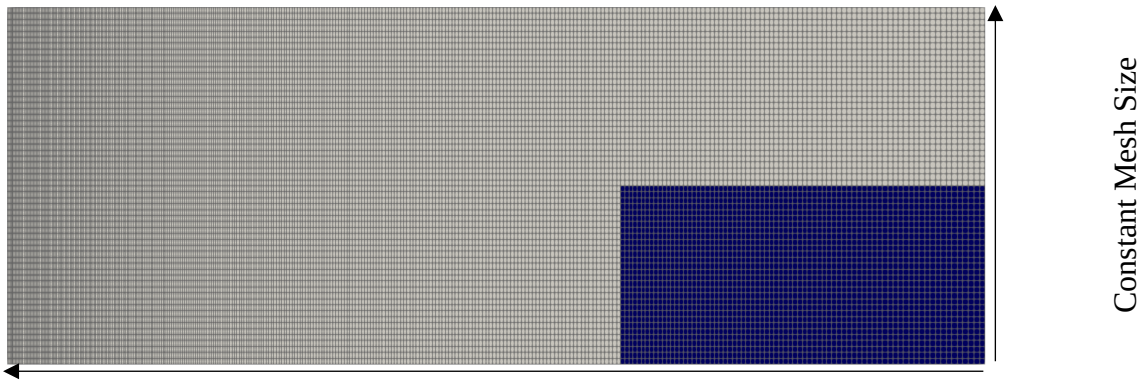

Figure 3.6. Representative mesh sizes in the x- and y-directions

The 2-D computational mesh, which lies on the x-z plane, is used for the oncoming investigations, which details will be presented in the following sections. Dimensions of the 2-D computational mesh are the same as the 3-D computational mesh except for the y-direction, which is excluded.

The computational mesh is categorized depending on the size of the largest cell dimensions as coarse mesh and fine mesh. Detailed information about the mesh sizes and corresponding cell numbers are listed in Table 3.3 for 3-D and 2-D computational meshes.

Table 3.3. Properties of computational mesh

Property	**3-D Coarse Mesh**	**3-D Fine Mesh**	**2-D Coarse Mesh**
Largest Cell Size	10 x 10 x 10 mm	5 x 5 x 5 mm	10 x 10 mm
Smallest Cell Size	2.5 x 10 x 10 mm	1.25 x 5 x 5 mm	2.5 x 10 mm
Number of Cells	289,800	2,318,400	19,320
Number of Faces	894,450	7,055,400	77,662

3.2.8 Boundary Conditions

Boundary conditions are essential to solve the RANS equations. Therefore, proper boundary conditions should be specified to solve these equations. Using the appropriate boundary conditions is vital since the results obtained are directly related to the selected boundary conditions. Boundary conditions representing the experimental setup are selected for the velocity field, pressure field and VOF-indicator function α and detailed explanations are given in this section.

In this study, no-slip boundary condition is applied to faces corresponding to tank walls for the velocity field, which indicates the relative velocity of the fluid to the boundary is equal to zero. On the other hand, for the atmosphere boundary condition in the velocity field, pressure inlet-outlet velocity is applied, a combination of pressure inlet velocity and inlet-outlet boundary conditions, meaning that if the pressure is known, inlet velocity is calculated from the flux value. The velocity value switches between a fixed value or zero gradient depending on the direction of the flow at the boundary.

Fixed flux pressure boundary condition is applied to the tank walls for pressure field, which allows setting the pressure gradient to a fixed value of flux that equals zero on the boundary provided by the specified velocity field boundary condition. The boundary condition on the atmosphere for the pressure field is set as total pressure, which means that the pressure value is calculated using the total pressure value p_0 at the boundary location.

For the VOF-indicator function α, zero gradient boundary condition is applied to the walls of the tank so that the value at the boundary is extrapolated from the nearest cell value, meaning that the quantity is developed enough, and the gradient is equal to zero in the direction normal to the boundary. Inlet outlet boundary condition is applied to the atmosphere for α which means the value is equal to a fixed value or has zero gradient depending on the flow direction.

3.3 Simulations

Firstly, the mesh independence study is performed. Then, 3-D and 2-D meshes are analyzed to study the 3-D effects on the impact pressure. After that, the effect of the maximum courant number on the results is examined. The gradient schemes and the compression flux is studied to investigate their effects on the results. Finally, the performance of the divergence schemes is investigated using different interpolation schemes for each parameter in the discretized conservation equations. Details of the process are given in the following sections, and the corresponding results of the study will be presented in the next chapter.

3.3.1 Mesh Independence

In numerical modelling studies, it is crucial to have model results independent of the computational mesh so that the accuracy of the results is reliable enough to make conclusions.

The mesh independence study is performed using the default interpolation schemes in the dam break tutorial for OpenFOAM, as shown in Table 3.4, on the 3-D computational mesh. Coarse and fine meshes whose properties are listed in Table 3.3 are generated. The results obtained from the fine mesh simulation are compared with the coarse one. Then, the 3-D coarse mesh is selected based on the results. Corresponding results of the study are given in Section 4.2.

Table 3.4. Default interpolation schemes for convective terms

Term Notation	**Numerical Scheme**
rhoPhi, U	linearUpwind
phi, alpha	vanLeer
phirb, alpha	linear

3.3.2 3-D Effects on the Impact Pressure

As Lobovský et al. (2014) mentioned in their study, it is possible to say that 3-D effects exist in dam break cases. However, their direct effect on the pressures applied to the structure remains unknown. Considering a rectangular obstacle facing violent impacts, applied pressure on the sides of the obstacle is different from those applied to the center, but this does not indicate that the pressure applied to the center is affected by the movement of the fluid around it. In order to see the difference between the pressure values obtained from 3-D and 2-D computational meshes, two simulations are prepared using the default schemes given in Table 3.4.

There is no significant difference observed between the 3-D and 2-D mesh results depending on the results given in detail in Section 4.3. Thus, due to computational constraints, the 2-D computational mesh is used for simulations for the rest of the investigation.

3.3.3 Effect of Maximum Courant Number

After the 3-D effects on the impact pressure study, the effect of the Courant-Friedrichs-Lewy (CFL) criterion is investigated in the simulations. In OpenFOAM, time steps can be fixed to a constant number or controlled by the Courant number for each time step. The initial step size is given for the simulation to start, and then the time step size is calculated so that the maximum Courant number is not exceeded using Equation 3.15.

$$Co = \frac{u\Delta t}{\Delta x} \leq Co_{max} \qquad \text{Equation 3.15}$$

Effect of the Courant number is investigated for the values ranging from 0.5 to 0.05. The results of the investigation are given in Section 4.4.

3.3.4 Effect of Gradient Schemes & Compression Flux Discretization

In previous simulations, a series of investigations are performed for different properties of the numerical model using the default scheme composition given in Sections 3.2.6 and 3.3.1.

In this section and the following, numerical schemes and their effects are investigated. In previous simulations, the default gradient scheme, Gauss and the default interpolation scheme linear are used for predictions for all gradients. However, this may cause instabilities in the model due to sharp changes in the velocity gradient since no limiter is applied to the interpolation scheme. A cell-limited linear interpolation scheme is applied to the velocity gradient to eliminate the possible instabilities. With this method, interpolation for the velocity gradient is limited with the values of neighboring cells, reducing the sharp changes in the estimation.

Deshpande et al. (2012) suggest using an alternative scheme on the discretization of compression flux term, the interfaceCompression scheme. As it is described in OpenFOAM User Guide (2019), the interfaceCompression scheme is based on the generic limited scheme, although it does not use NVD or TVD functions. Basically, it applies interface compression to the phase fraction distribution so that the value is set as 1 if it is above 0.5 or else it is set to 0.

Results for the effect of gradient schemes and the interpolation scheme for compression flux are given in Section 4.5.

3.3.5 Effect of Divergence Schemes

Finally, the effect of the interpolation schemes for the convective term is investigated in this section. The numerical schemes listed in Table 3.2 are used on the “rhoPhi, U” term to determine the performance. All other parameters are kept constant for a controlled performance test.

27 different interpolation schemes are evaluated for the discretization of the “rhoPhi, U” term and the best three options among those are further investigated for the following discretization, the “phi, alpha” term, resulting in a total of 81 simulations and 54 different numerical scheme combinations.

Interpolation schemes for the “phi, alpha” term discretization are the same as listed in Table 3.2, deducting “V” schemes since they cannot be used for this term. Once again, the best three options among these schemes are also selected for evaluation.

Results obtained for the best three options for the “rhoPhi, U” term and the “phi, alpha” term are given in Sections 4.6.1 and 4.6.2, respectively. Results of all schemes are given in Appendix A for the “rhoPhi, U” term and in Appendix B for the “phi, alpha” term.

CHAPTER 4

RESULTS

Results of the simulations given in Section 3.3 and the methodology used in the analysis of the results are presented in this chapter.

4.1 Analysis of Results

A series of simulations are used to investigate the performance of different numerical schemes. Simulation time is selected as 0.7 seconds corresponding to approximately 4 in terms of dimensionless time. The time is non-dimensionalized using the relation in Equation 4.1,

$$T = \frac{t}{\sqrt{H/g}} \qquad \text{Equation 4.1}$$

Determination of the simulation time is based on the impact zone observed at sensor locations. The impact zone is determined using the methodology described in Section 2.1 for the experimental results based on the median values where the highest probability of occurrence lies. For Sensor-1 and Sensor-2 locations, a clear impact zone is observed in the pressure-time histories, while Sensor-3 and Sensor-4 locations are considered out of the impact zone depending on the pressure-time histories obtained at sensor locations.

The performances of the simulations are evaluated and compared using error analysis. Percent error (PE) is used for the peak pressure value. Normalized root mean square error (NRMSE) and normalized mean absolute error (NMAE) are used for the overall results. For Sensor-1 and Sensor-2 locations, the overall result comparison is performed within the impact zone ($2.44 < T < 3.16$ for Sensor-1). However, the comparison is performed for Sensor-3 and Sensor-4 locations, starting

from the beginning of the rise zone to the end of the simulation time ($2.36 < T < 4$ for Sensor-3 and Sensor-4), since no impact zone is observed at these locations.

Percent error is calculated using Equation 4.2,

$$PE = \left| \frac{y_{model} - y_{exp}}{y_{exp}} \right| \times 100\% \qquad \text{Equation 4.2}$$

In Equation 4.2, y_{exp} is the value obtained in reference experiment and y_{model} is the value obtained from the numerical model.

Root mean square error is calculated using Equation 4.3 and normalized using Equation 4.4,

$$RMSE = \sqrt{\frac{\sum_{i=1}^{N} \left(y_{i,model} - y_{i,exp}\right)^2}{N}} \qquad \text{Equation 4.3}$$

$$NRMSE = \frac{RMSE}{\overline{y_{exp}}} \qquad \text{Equation 4.4}$$

In Equations 4.3 and 4.4, $y_{i,exp}$ and $y_{i,model}$ correspond to the ith value of the reference experiment and the numerical model, respectively. N is the total number of data points. $\overline{y_{exp}}$ is the mean value of the reference experimental data.

Mean absolute error is calculated using Equation 4.5 and normalized using Equation 4.6,

$$MAE = \frac{\sum_{i=1}^{N} \left| y_{i,model} - y_{i,exp} \right|}{N} \qquad \text{Equation 4.5}$$

$$NMAE = \frac{MAE}{\sigma_{exp}} \qquad \text{Equation 4.6}$$

In Equation 4.6, σ_{exp} is the standard deviation of the reference experimental data.

Median values obtained from the pressure transducers in the physical experiment are used to analyze the results obtained from the simulations.

4.2 Mesh Independence

The mesh independence study is performed using the default interpolation schemes for coarse and fine meshes whose properties are listed in Table 3.3. The results obtained at the Sensor-1 location are used for the error analysis due to the better representation of impact pressure at its location. First, the peak pressure values and overall results within the impact zone are determined for the coarse mesh. Then, results obtained from the fine mesh are compared with the results of the coarse mesh. Corresponding results are listed in Table 4.1.

Table 4.1. Comparison of coarse and fine meshes

Error Type	**Difference in Fine Mesh**
Percent Error (PE)	0.52%
Normalized Root Mean Square Error (NRMSE)	0.3491
Normalized Mean Absolute Error (NMAE)	0.1610

The percent error for the fine mesh is 0.52%, while the NMAE value is 0.1610, which indicates that the peak pressure prediction performance is in good agreement and the overall result of the coarse mesh is acceptable even though the NRMSE value obtained deviates more. Pressure-time histories for both cases are given in Figure 4.1. In the figure, the upper bound of the confidence range is the 97.5% percentile, and the lower bound is the 2.5% percentile. A similar trend between the cases is observed. The coarse mesh is selected for the investigation due to the high computational demand in the fine mesh and favorable error margins between the coarse and fine meshes.

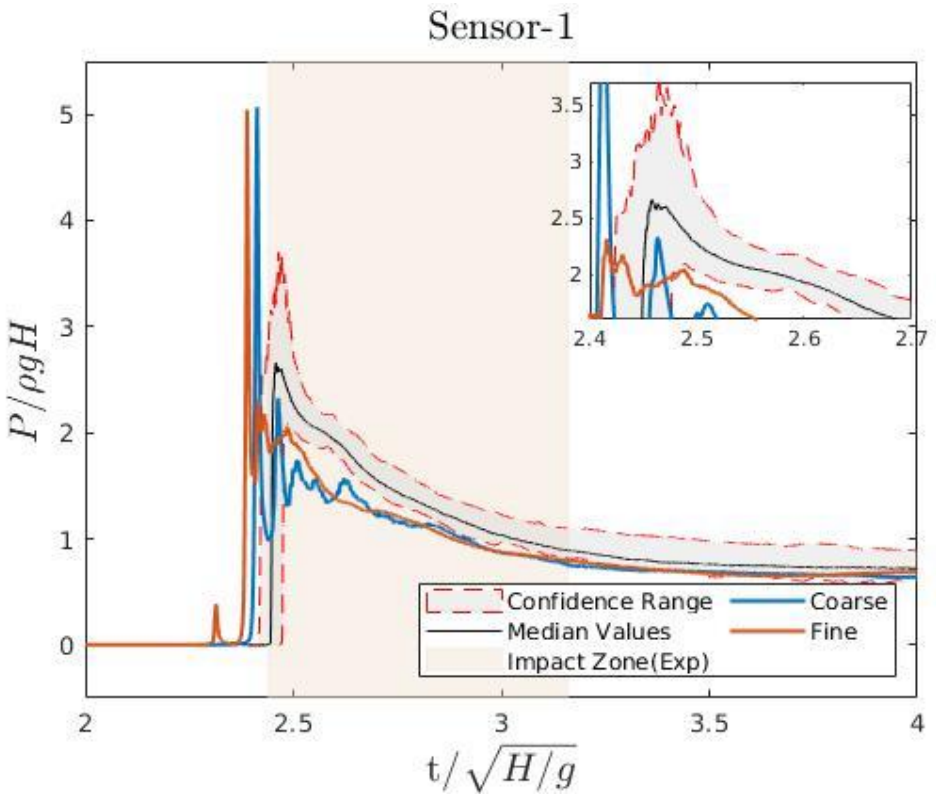

Figure 4.1. Pressure-time histories for coarse and fine meshes at Sensor-1

4.3 3-D Effects on the Impact Pressure

Two simulations are prepared using the default interpolation schemes for 3-D and 2-D computational meshes. Then, results obtained from the 2-D mesh are compared with the results of the 3-D mesh regarding the peak pressure values and overall results within the impact zone described in Section 4.1. Corresponding results for the comparison of 3-D and 2-D computational meshes are given in Table 4.2.

Table 4.2. Comparison of 3-D and 2-D computational meshes

Error Type	**Difference in 2-D Computational Mesh**
Percent Error (PE)	3.93%
Normalized Root Mean Square Error (NRMSE)	0.2243
Normalized Mean Absolute Error (NMAE)	0.1299

According to the results in Table 4.2, there is a slight difference between the two models, as indicated in Section 3.1.1. The maximum variation for peak pressure prediction between the models is 3.93%, while the computational time is reduced by almost 90% from 1478 seconds to 162 seconds, using the 2-D computational mesh. Hence, the 2-D computational mesh is used for the performance tests.

4.4 Effect of Maximum Courant Number

The effect of the Courant number is investigated for the values ranging from 0.5 to 0.05 using the default interpolation schemes. Six simulations are prepared for this purpose. Then, the results obtained from these are compared with the reference experimental data regarding the peak pressure values and overall results within the impact zone. The results of the investigation are given in Table 4.3.

The maximum Courant number is selected for the optimum results instead of the best result so that the accuracy of the simulation can be increased without increasing the computational time drastically.

Table 4.3. Comparison of the performances based on Co_{max} value

Error Type	**Courant Number**					
	0.5	***0.4***	***0.3***	***0.2***	***0.1***	***0.05***
PE Sensor-1	83.09%	98.37%	96.97%	51.50%	50.51%	69.30%
PE Sensor-2	60.06%	67.22%	52.08%	15.90%	19.81%	36.77%
PE Sensor-3	10.62%	11.88%	11.04%	9.93%	11.84%	6.45%
PE Sensor-4	28.59%	26.38%	26.08%	25.03%	26.62%	25.55%
NRMSE Sensor-1	0.2961	0.2912	0.2805	0.2716	0.2680	0.2592
NRMSE Sensor-2	0.3980	0.3951	0.3757	0.3530	0.3271	0.3376
NRMSE Sensor-3	0.3045	0.3061	0.2975	0.3131	0.2821	0.2546
NRMSE Sensor-4	0.2128	0.2158	0.2180	0.2287	0.2161	0.2028
NMAE Sensor-1	0.6969	0.6410	0.6268	0.6219	0.6372	0.5728
NMAE Sensor-2	0.4723	0.4394	0.4150	0.4154	0.4075	0.4290
NMAE Sensor-3	0.4164	0.4483	0.4407	0.4430	0.3837	0.3842
NMAE Sensor-4	0.2125	0.2413	0.2396	0.2365	0.2208	0.2255

Based on the results given in Table 4.3, $Co_{max} = 0.1$ is the best option to predict the peak pressure value depending on the percent error obtained, while $Co_{max} = 0.05$ is the best option for more accurate overall results depending on the NRMSE and NMAE values at the Sensor-1.

$Co_{max} = 0.1$ is selected for investigating numerical scheme performances at the slight expense of overall results.

Pressure-time histories of the simulation with $Co_{max} = 0.1$ are given in Figure 4.2.

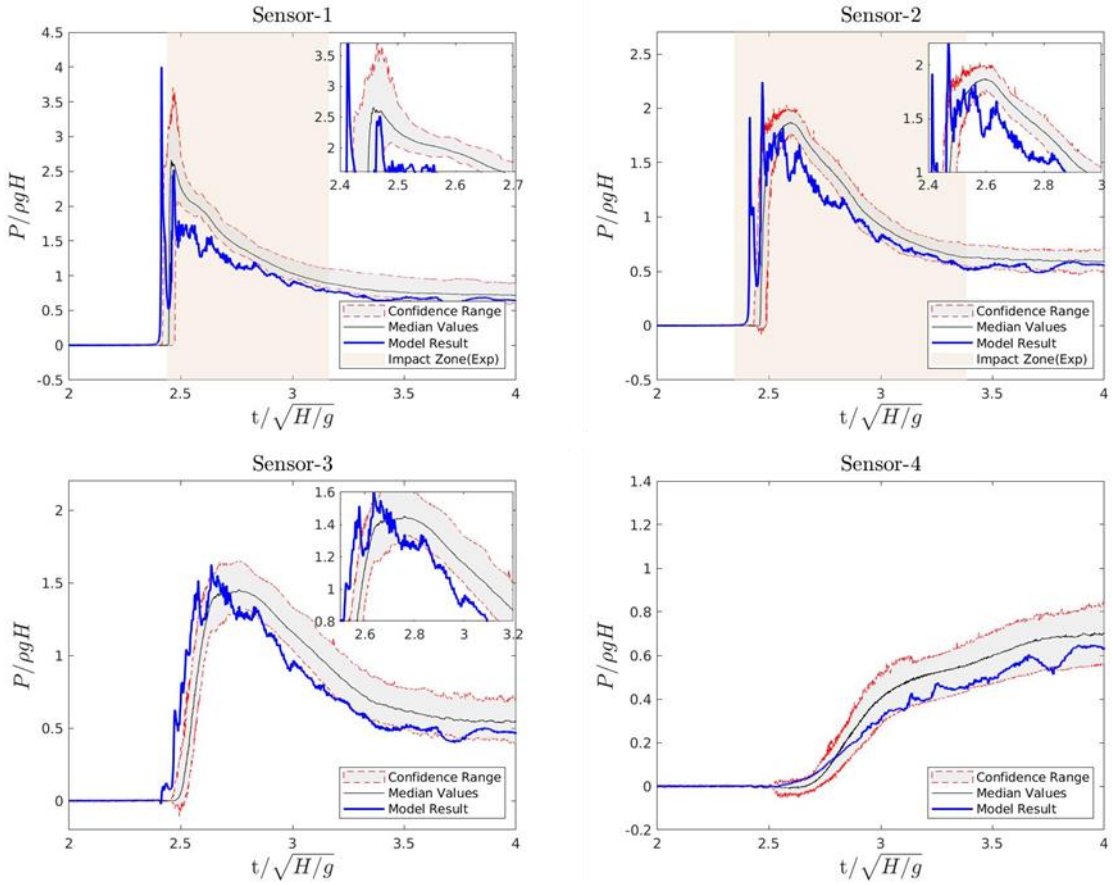

Figure 4.2. Pressure-time histories obtained with $Co_{max} = 0.1$

4.5 Effect of Gradient Schemes & Compression Flux Discretization

First, the effect of the gradient scheme is investigated using a cell-limited linear interpolation scheme, which is applied to the velocity gradient. Then, the interfaceCompression scheme is used for the discretization of compression flux. Finally, the performance of these two schemes combined is determined. Results obtained from these three simulations are compared with reference experimental data regarding the peak pressure values and overall results within the impact zone. Corresponding results are given in Table 4.4 with the results of the default interpolation scheme to assess the change in performance.

Table 4.4. Comparison of the performances of gradient scheme & compression flux discretization

Error Type	Cases			
	Default Schemes	**Gradient Scheme**	**Compression Flux Discretization**	**Schemes Combined**
PE Sensor-1	50.51%	38.32%	8.34%	26.63%
PE Sensor-2	19.81%	22.87%	2.51%	12.33%
PE Sensor-3	11.84%	4.76%	4.73%	10.47%
PE Sensor-4	26.62%	55.58%	27.32%	56.33%
NRMSE Sensor-1	0.2680	0.2955	0.3051	0.2688
NRMSE Sensor-2	0.3271	0.2851	0.3147	0.2742
NRMSE Sensor-3	0.2821	0.2392	0.2929	0.2337
NRMSE Sensor-4	0.2161	0.5994	0.2280	0.6194
NMAE Sensor-1	0.6372	0.3328	0.6901	0.3411
NMAE Sensor-2	0.4075	0.3821	0.4020	0.3731
NMAE Sensor-3	0.3837	0.4013	0.4055	0.3926
NMAE Sensor-4	0.2208	0.7690	0.2224	0.7182

In Table 4.4, it is seen that the results are generally better with respect to the default interpolation scheme case except for the Sensor-4 location which the performance drastically drops with the gradient scheme. Despite the decreased performance for Sensor-4, a general improvement is observed for Sensor-1, Sensor-2, and Sensor-3. The default interpolation scheme is modified so that the cell limited gradient scheme is applied to the velocity gradient. The interfaceCompression scheme is used in compression flux discretization for further investigations at the expense of accuracy in peak pressure prediction.

Pressure-time histories for the modified case are given in Figure 4.3. A good agreement for the general trend is observed at the Sensor-1 location, while the pressure values slightly differ in the decay zone at the Sensor-2 location. Peak pressure value is underestimated at Sensor-3 location, but the results are in good agreement with the confidence range of the experimental results. However, at the Sensor-4 location, pressure is highly underestimated. The reason might be the different flow characteristics at this location, where the pressure is due to run up instead of the direct impact of the fluid. Since this study is focused on the impact pressures, this deficiency is considered acceptable and left for future work.

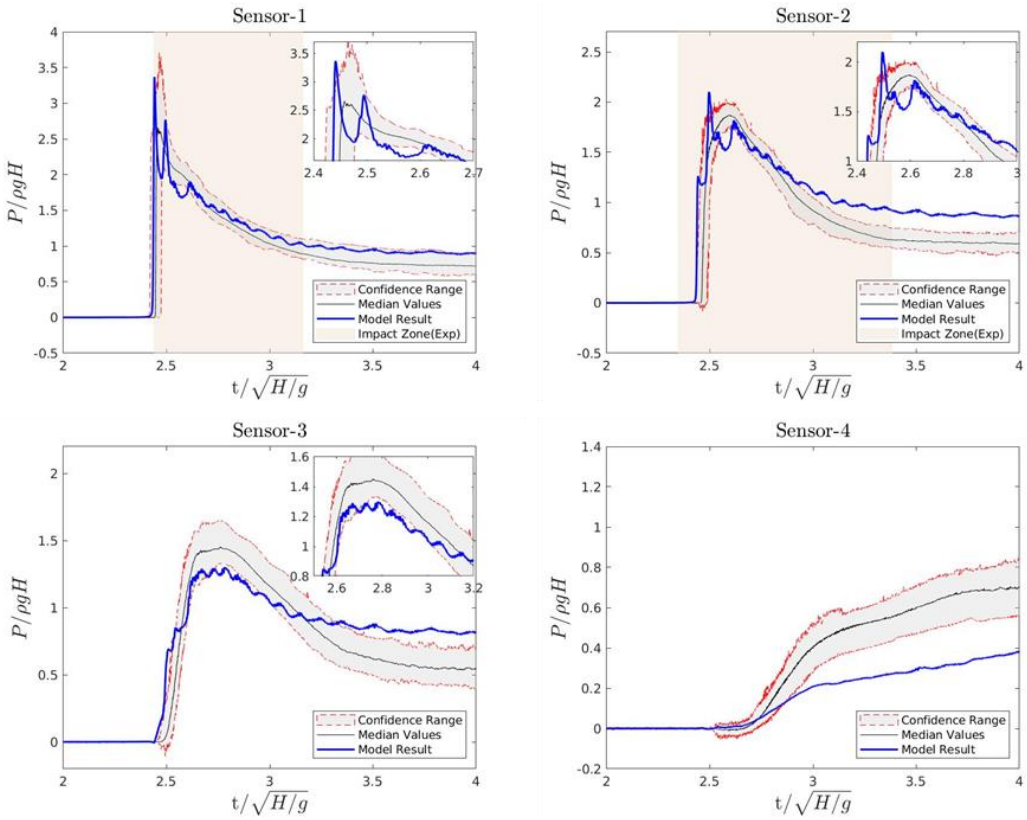

Figure 4.3. Pressure-time histories with gradient scheme & compression flux discretization changes

4.6 Effect of Divergence Schemes

First, the numerical schemes listed in Table 3.2 are used on the “rhoPhi, U” term discretization to determine the performance of the schemes, while all other parameters are kept constant as indicated in Table for a controlled performance test. Then, the best three options among those are selected regarding the peak pressure values and overall results within the impact zone. These selections include one for the best percent error, one for the best overall results in terms of NRMSE, and one for NMAE. The selected simulations are further investigated for the following discretization, the “phi, alpha” term. Once again, the best three options among these schemes are also selected to evaluate the performance of the scheme couples.

Table 4.5. Selected parameters to be kept constant

Parameter	**Selection**
Computational Mesh Resolution	Coarse Mesh
Computational Mesh Dimension	2-D Mesh
Maximum Courant Number	0.1
Gradient Scheme	Cell limited linear
Discretization of Compression Flux	Interface Compression

4.6.1 Effect of the Discretization of the Convective Terms in Momentum Equation

The numerical schemes listed in Table 3.2 are applied to the “rhoPhi, U” term, while the default interpolation scheme for the “phi, alpha” term is kept constant. Results obtained from these simulations are compared with reference experimental data regarding the peak pressure values and overall results within the impact zone. Depending on the results of simulations with different numerical schemes, the best three options are selected based on PE, NRMSE and NMAE values at the Sensor-1

location, which are limitedLinear 0.4, SuperBee and linearUpwind schemes, respectively. Corresponding results of these three simulations are given in Table 4.6. The rest of the results are given in Appendix A.

Table 4.6. Comparison of the performances based on the “rhoPhi, U” term discretization

Error Type	**Cases**		
	Limited Linear 0.4	**SuperBee**	**Linear Upwind**
PE Sensor-1	3.22%	5.10%	26.63%
PE Sensor-2	1.81%	7.82%	12.33%
PE Sensor-3	9.07%	2.02%	10.47%
PE Sensor-4	57.67%	48.94%	56.33%
NRMSE Sensor-1	0.2431	0.1891	0.2688
NRMSE Sensor-2	0.3324	0.3020	0.2742
NRMSE Sensor-3	0.2761	0.2568	0.2337
NRMSE Sensor-4	0.7039	0.6345	0.6194
NMAE Sensor-1	0.4911	0.4095	0.3411
NMAE Sensor-2	0.4478	0.3917	0.3731
NMAE Sensor-3	0.4452	0.4023	0.3926
NMAE Sensor-4	0.7511	0.6842	0.7182

The limited linear interpolation scheme with a coefficient of 0.4 is the best option to determine the peak pressure value, while its performance is significantly lower with respect to other options considering the NMAE. The NRMSE level of the case is also acceptable. The SuperBee interpolation scheme is the best option for overall results in terms of NRMSE, while relatively low accuracy is obtained with the NMAE analysis. On the other hand, peak pressure value accuracy is higher than in most cases, making the scheme a reasonably good option. The linear upwind interpolation scheme is the best option for overall results in terms of NMAE, while

the NRMSE results show that the lowest accuracy is obtained among these three alternatives. Besides that, the peak pressure value obtained using this scheme is notably lower than the other two options.

Pressure time histories obtained from numerical models at Sensor-1, Sensor-2, Sensor-3 and Sensor-4 locations are given in Figure 4.4, Figure 4.5 and Figure 4.6 for limited linear interpolation scheme with a coefficient of 0.4, SuperBee and linear upwind interpolation schemes, respectively. It should be once again noted that the numerical schemes mentioned above are only applied to the "rhoPhi, U" term discretization and the "phi, alpha" term discretization is kept constant as it is in the default interpolation scheme case where van Leer interpolation scheme is applied.

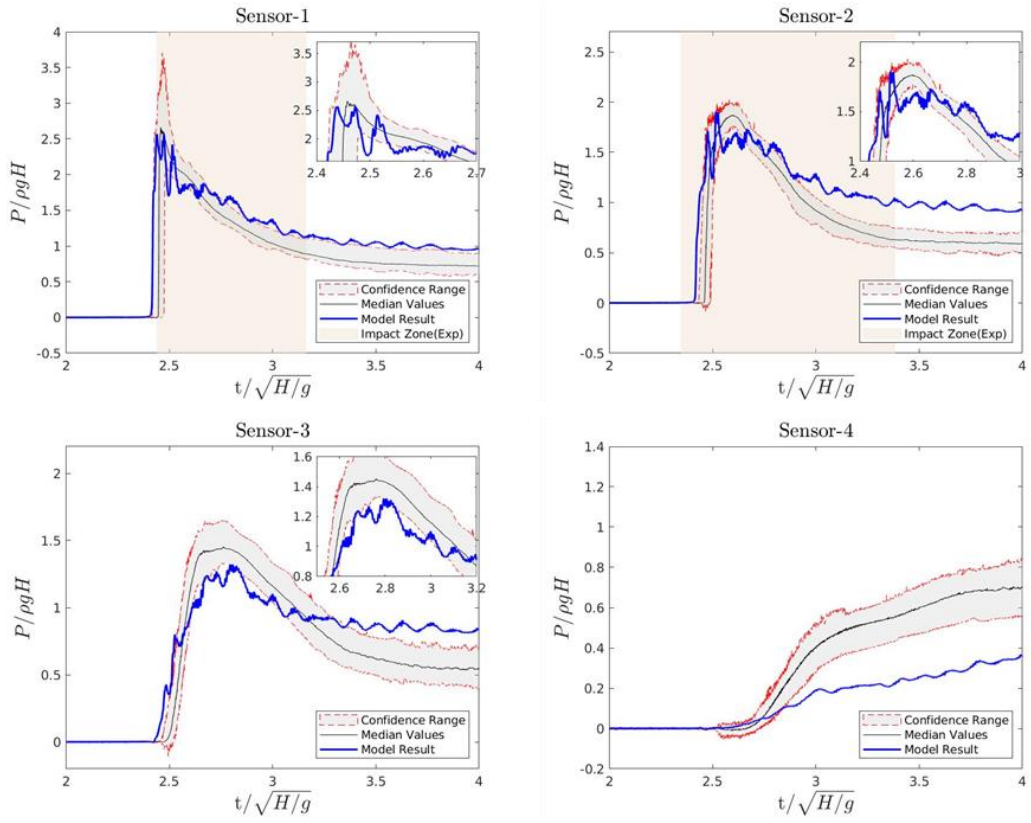

Figure 4.4. Pressure-time histories for limited linear 0.4 scheme applied to the "rhoPhi, U" term discretization

According to the pressure-time histories in Figure 4.4, a good agreement between the simulation and the experimental results for the rise part of the impact zone is observed at the Sensor-1 location with good accuracy of the peak pressure value. After the impact zone, pressure values are overestimated for the rest of the simulation, causing discrepancies in the overall result. However, considering pressure values are within the confidence range for the experimental result, it can be said that the numerical scheme is acceptable for studies where the peak pressure value determination is a great concern.

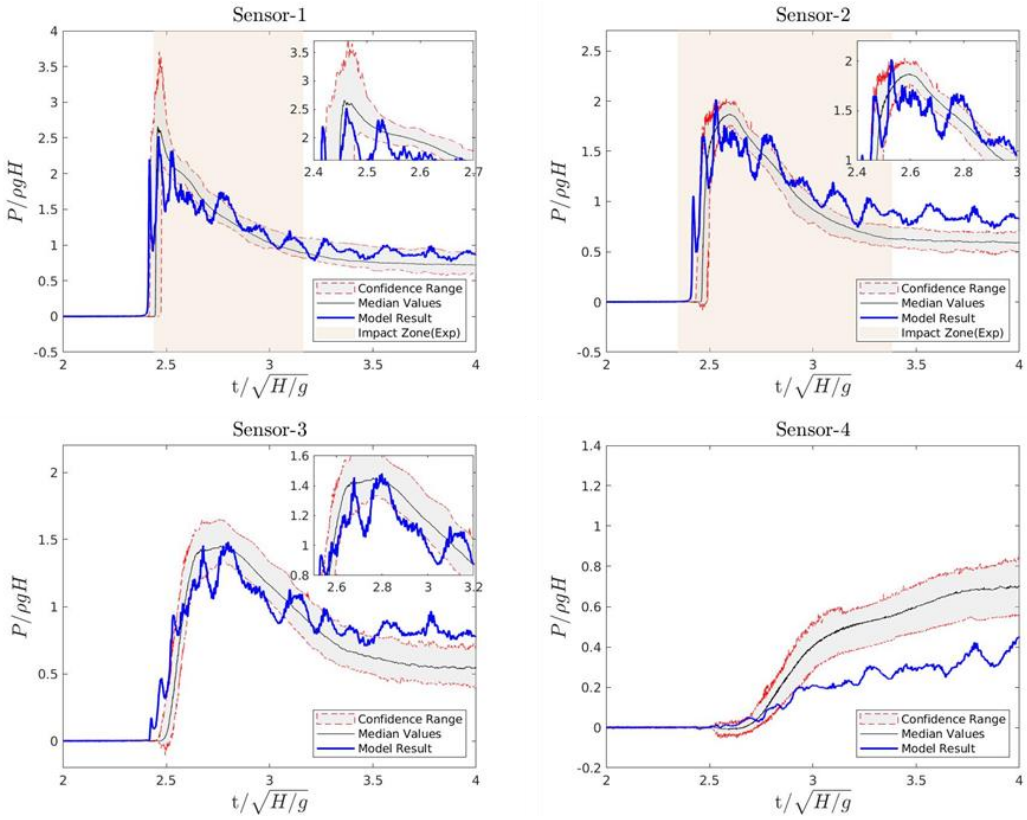

Figure 4.5. Pressure-time histories for SuperBee scheme applied to the “rhoPhi, U” term discretization

In Figure 4.5, pressure values obtained at the Sensor-1 location slightly deviate throughout the simulation, and it is not possible to say that the overall result follows a specific behavior. Instead, there are several points where over and underestimations are observed. These deviations around the median values result in a lower NRMSE,

while some deficiencies are seen both in the rise and decay parts of the impact zone. Furthermore, the scheme gives a good agreement on the peak pressure value slightly lower than the previous scheme. Thus, it can be a good option for studies where both peak pressure and pressure values in the impact zone are great concerns.

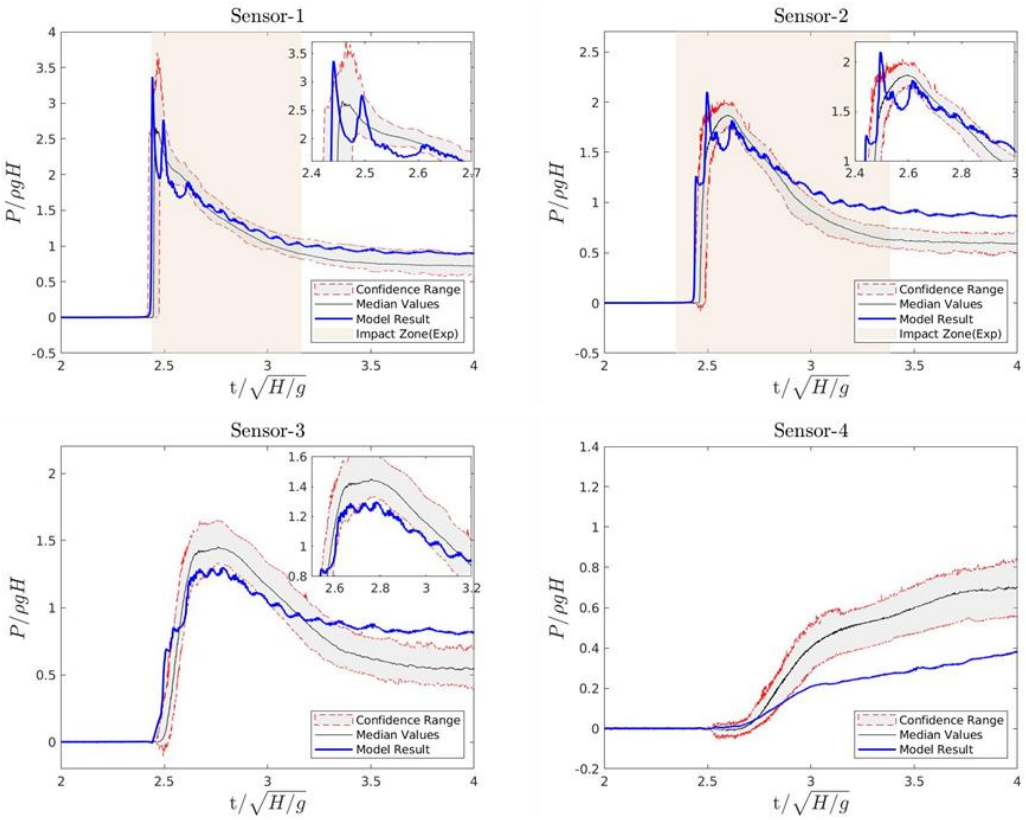

Figure 4.6. Pressure-time histories for linear upwind scheme applied to the "rhoPhi, U" term discretization

Pressure time histories in Figure 4.6 show a good agreement in the decay part of the impact zone, and the smoothest curves are observed in this numerical scheme option. However, the peak pressure value is highly overestimated with respect to the other two scheme options. Considering the high accuracy obtained within the impact zone at the Sensor-1 location, this scheme is a good option for studies where the overall result is a great concern instead of accurate impact pressure determination.

4.6.2 Effect of the Discretization of the Convective Term in VOF-Advection Equation

27 different interpolation schemes are evaluated for the discretization of the “rhoPhi, U” term and the best three options, which are limited linear interpolation scheme with a coefficient of 0.4, SuperBee and linear upwind interpolation schemes, are selected to be investigated further for the following discretization, the “phi, alpha” term.

Interpolation schemes for the “phi, alpha” term discretization are similar to those in Table 3.2, deducting “V” schemes since they cannot be used for this term. The updated list of the numerical schemes considered for the “phi, alpha” term discretization is given in Table 4.7.

Table 4.7. Numerical scheme list considered for the “phi, alpha” term discretization

#	**Numerical Scheme**	#	**Numerical Scheme**
01	linear	10	Minmod
02	midPoint	11	vanLeer
03	upwind	12	MUSCL
04	linearUpwind	13	QUICK
05	limitedLinear, Coeff = 0.2	14	UMIST
06	limitedLinear, Coeff = 0.4	15	vanAlbada
07	limitedLinear, Coeff = 0.6	16	SuperBee
08	limitedLinear, Coeff = 0.8	17	SFCD
09	limitedLinear, Coeff = 1.0	18	Gamma

The numerical schemes listed in Table 4.7 are applied to the “phi, alpha” term, while the previously selected schemes for the “rhoPhi, U” term are kept constant. Results obtained from these simulations are compared with reference experimental data regarding the peak pressure values and overall results within the impact zone.

Depending on the results of simulations with different numerical schemes, the best three options are selected based on PE, NRMSE and NMAE values at the Sensor-1 location.

The limited linear interpolation scheme with a coefficient of 0.4 is evaluated first. The results of the best three alternatives depending on PE, NRMSE and NMAE values at Sensor-1 location are listed in Table 4.8.

Table 4.8. Comparison of the performances based on the "phi, alpha" term discretization with limitedLinear 0.4 "rhoPhi, U" discretization

Error Type	**Cases**		
	Limited Linear 0.4	**Upwind**	**Gamma**
PE Sensor-1	2.29%	14.11%	3.54%
PE Sensor-2	2.02%	6.28%	2.01%
PE Sensor-3	9.40%	13.30%	13.06%
PE Sensor-4	58.74%	59.86%	60.13%
NRMSE Sensor-1	0.2136	0.1739	0.2055
NRMSE Sensor-2	0.3069	0.2708	0.3161
NRMSE Sensor-3	0.2618	0.2731	0.2678
NRMSE Sensor-4	0.7059	0.7038	0.7061
NMAE Sensor-1	0.4443	0.3981	0.4380
NMAE Sensor-2	0.3977	0.3926	0.4177
NMAE Sensor-3	0.4238	0.4514	0.4352
NMAE Sensor-4	0.7316	0.7299	0.7236

According to the results obtained in Table 4.8, the limited linear interpolation scheme with a coefficient of 0.4 further improves the peak pressure prediction accuracy, also boosting the results in both NRMSE and NMAE. However, a great increase in the accuracy of overall results is obtained using the upwind interpolation scheme

depending on NRMSE and NMAE, which shows the scheme is the best option for both. On the other hand, the Gamma interpolation scheme is the follow-up for both NMRSE and NMAE, while it also increases the accuracy of the peak pressure determination significantly. Thus, the Gamma scheme is included in the best alternatives among those. Pressure-time histories at Sensor-1 location for each alternative are given in Figure 4.7.

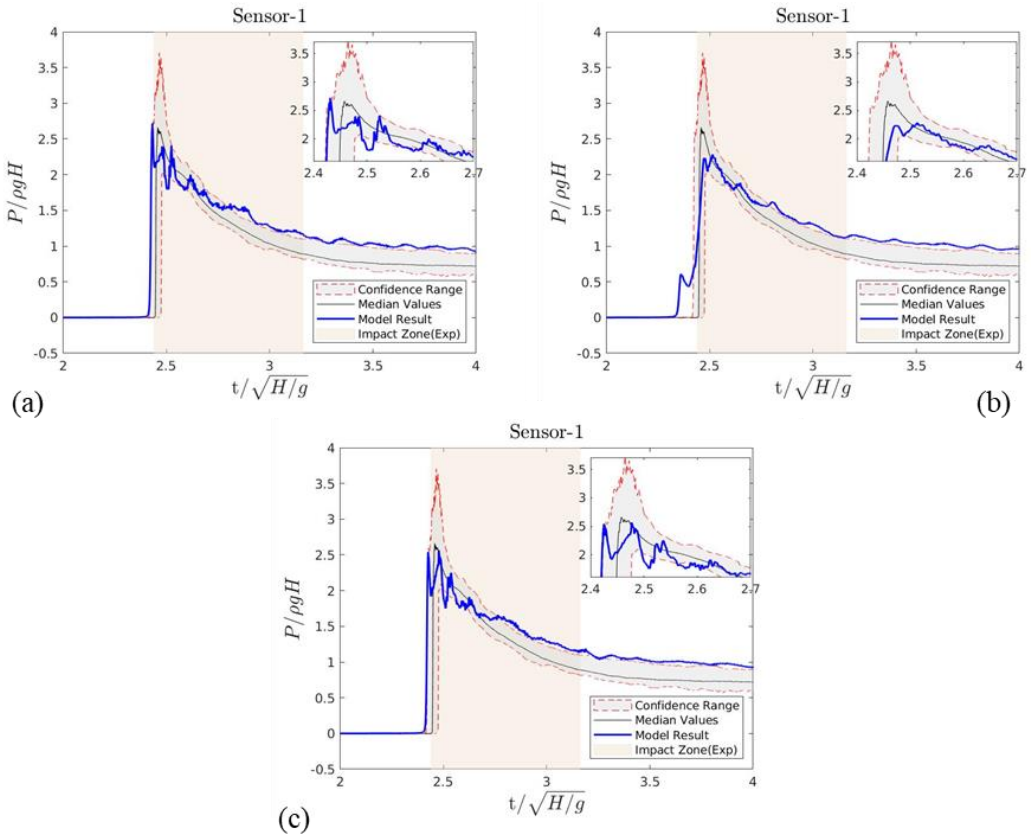

Figure 4.7. Pressure-time histories at Sensor-1 for limited linear 0.4 scheme applied to the “rhoPhi, U” term discretization with the “phi, alpha” term discretization couple (a). limited linear 0.4 (b). upwind (c). Gamma

Then, the SuperBee scheme is evaluated. The results of the best three alternatives depending on PE, NRMSE and NMAE values at Sensor-1 location are listed in Table 4.9.

Table 4.9. Comparison of the performances based on the “phi, alpha” term discretization with SuperBee “rhoPhi, U” discretization

Error Type	**Cases**		
	Gamma	**van Leer**	**Minmod**
PE Sensor-1	0.50%	5.10%	5.70%
PE Sensor-2	2.97%	7.82%	4.44%
PE Sensor-3	2.64%	2.02%	14.76%
PE Sensor-4	42.31%	48.94%	52.43%
NRMSE Sensor-1	0.2217	0.1891	0.2147
NRMSE Sensor-2	0.2545	0.3020	0.2640
NRMSE Sensor-3	0.2127	0.2568	0.2327
NRMSE Sensor-4	0.6097	0.6345	0.6260
NMAE Sensor-1	0.3322	0.4095	0.3562
NMAE Sensor-2	0.2953	0.3917	0.3548
NMAE Sensor-3	0.3195	0.4023	0.3707
NMAE Sensor-4	0.5934	0.6842	0.6176

According to the results obtained in Table 4.9, the Gamma scheme significantly improves the peak pressure determination performance with a value of only 0.5% deviation. However, performance on the overall result is significantly reduced considering the NRMSE making the scheme combination undesirable since the SuperBee scheme is further investigated based on the NRMSE results. The van Leer interpolation scheme remains as the best option for overall results based on the NRMSE criterion. On the other hand, the Minmod scheme creates a third option since the overall performance based on the NMAE results is higher than the van Leer scheme, while the peak pressure determination performance is approximately the same. There is a slight decrease in the overall results depending on the NRMSE, but these results are still acceptable considering this option is an alternative between

Gamma and van Leer schemes. Pressure-time histories at Sensor-1 location for each alternative are given in Figure 4.8.

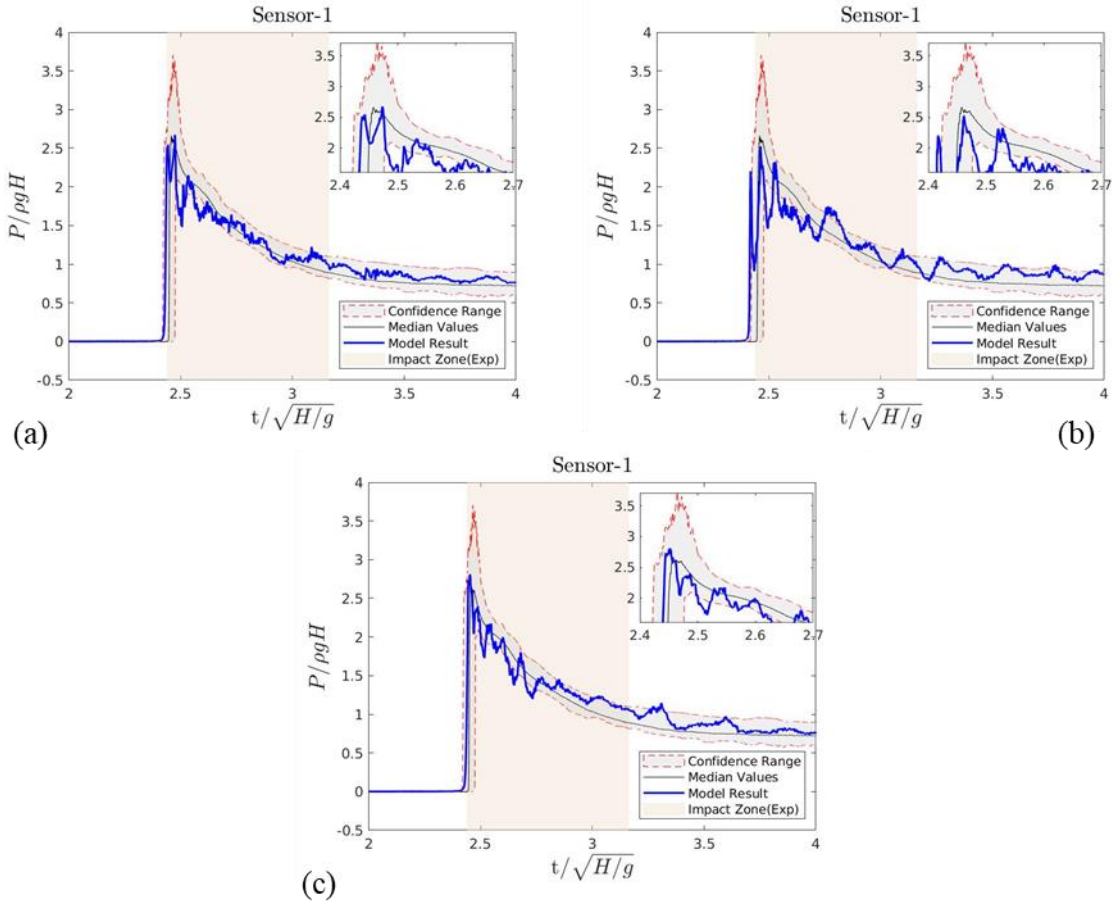

Figure 4.8. Pressure-time histories at Sensor-1 for SuperBee scheme applied to the "rhoPhi, U" term discretization with the "phi, alpha" term discretization couple (a). Gamma (b). van Leer (c). Minmod

Finally, the linear upwind scheme is evaluated. The results of the best three alternatives depending on PE, NRMSE and NMAE values at Sensor-1 location are listed in Table 4.10.

Table 4.10. Comparison of the performances based on the “phi, alpha” term discretization with linear upwind “rhoPhi, U” discretization

Error Type	Cases		
	Linear Upwind	**Upwind**	**Limited Linear 0.2**
PE Sensor-1	2.77%	18.25%	16.11%
PE Sensor-2	17.49%	6.18%	3.73%
PE Sensor-3	7.67%	9.44%	8.69%
PE Sensor-4	56.42%	58.31%	56.32%
NRMSE Sensor-1	0.2404	0.1818	0.2514
NRMSE Sensor-2	0.2742	0.2842	0.2674
NRMSE Sensor-3	0.2413	0.2878	0.2294
NRMSE Sensor-4	0.6221	0.6465	0.6175
NMAE Sensor-1	0.3349	0.3343	0.3065
NMAE Sensor-2	0.3611	0.3711	0.3501
NMAE Sensor-3	0.3928	0.4421	0.3795
NMAE Sensor-4	0.6959	0.6664	0.6922

According to the results obtained in Table 4.10, the linear upwind coupled with the linear upwind scheme gives the best result on the peak pressure determination with only a 2.77% difference between the simulation and the experimental results. Considering the initial results for the linear upwind scheme, a significant increase in the performance is observed while NRMSE and NMAE results also slightly increase. The upwind scheme further increases the overall performance in terms of NRMSE, while the limited linear interpolation scheme with a coefficient of 0.2 increases it in terms of NMAE. Besides, there is a slight increase in peak pressure performance on both. The linear upwind scheme is the best alternative considering both peak pressure and the overall performance of the scheme. Pressure-time histories at Sensor-1 location for each alternative are given in Figure 4.9.

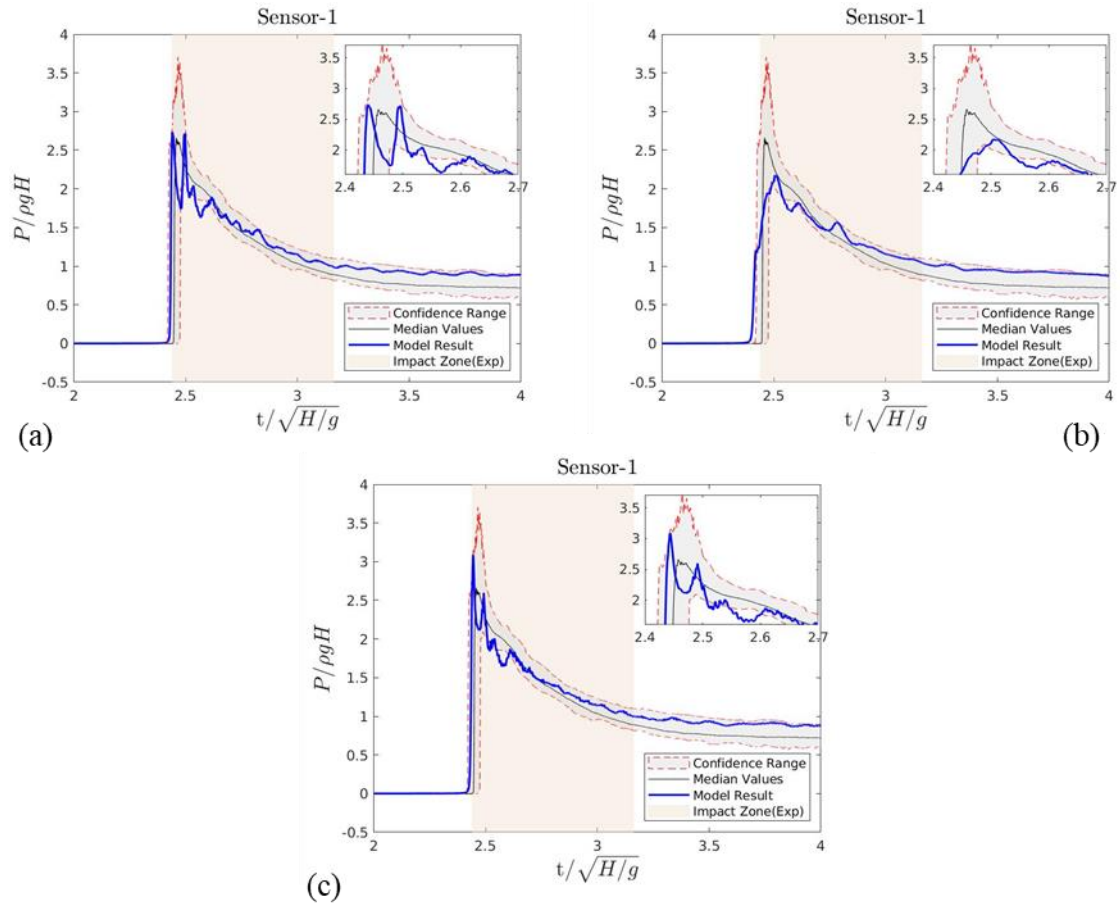

Figure 4.9. Pressure-time histories at Sensor-1 for linear upwind scheme applied to the "rhoPhi, U" term discretization with the "phi, alpha" term discretization couple (a). linear upwind (b). upwind (c). limited linear 0.2

The rest of the results for each of the three different "rhoPhi, U" discretization is given in Appendix B.

The results obtained from the investigation are compared with the default interpolation scheme at the Sensor-1 location in Table 4.11 for closure.

Table 4.11. Comparison of the performances of the investigated numerical schemes with default interpolation schemes (the first scheme refers to the “rhoPhi, U” term discretization, and the second scheme refers to the “phi, alpha” term discretization)

Case	**Error Type**		
	PE Sensor-1	**NRMSE Sensor-1**	**NMAE Sensor -1**
Default Schemes	50.51%	0.2680	0.6372
Limited Linear 0.4 Limited Linear 0.4	2.29%	0.2136	0.4443
Limited Linear 0.4 Upwind	14.11%	0.1739	0.3981
Limited Linear 0.4 Gamma	3.54%	0.2055	0.4380
SuperBee Gamma	0.50%	0.2217	0.3322
SuperBee vanLeer	5.10%	0.1891	0.4095
SuperBee Minmod	5.70%	0.2147	0.3562
Linear Upwind Linear Upwind	2.77%	0.2404	0.3349
Linear Upwind Upwind	18.25%	0.1818	0.3343
Linear Upwind Limited Linear 0.2	16.11%	0.2514	0.3065

Based on the results in Table 4.11, the SuperBee and Gamma scheme couple yields the best result on the peak pressure prediction, while applying the linear upwind scheme with a coefficient of 0.4 to both terms is the follow-up. On the other hand, the limited linear scheme with a coefficient of 0.4 coupled with the upwind scheme significantly reduces errors in terms of NRMSE. The linear upwind scheme coupled with the linear upwind scheme results in a major improvement in terms of NMAE, while the peak pressure prediction performance is relatively high.

CHAPTER 5

CONCLUSION

The primary focus of this thesis study is the evaluation of the effects of numerical schemes on the computation of impact pressure prediction. A numerical modelling study is performed using interFoam solver based on the OpenFOAM CFD Library. The wave-structure interaction during dam break event is investigated with different numerical schemes to assess the performances of the schemes. The performance tests are evaluated using the peak pressure prediction and the overall pressure prediction accuracies, comparing the numerical results with the measurements from a physical model experiment. The performance assessment is conducted in terms of percent error, normalized root mean square error and normalized mean absolute error.

The numerical modelling process is summarized (Chapter 3). The information about the reference physical model experiment is given. The numerical modelling study is explained in detail, and an introduction to numerical solution algorithms and numerical schemes is presented. Numerical simulations used to investigate the effects of the numerical schemes are introduced. A total of 81 different simulations have been performed, including 54 different combinations.

Results of the simulations and the methodology used in the analysis of the results are presented (Chapter 4). Although the discussions and evaluations are given previously at the end of each section, the conclusions of the study are summarized below:

- 3-D effects on the impact pressure prediction are investigated using two simulations performed in 3-D and 2-D computational domains. The results of the investigation indicate that there is a slight difference between these, where the variation between the models is 3.93%, while the computational time is reduced by almost 90% using the 2-D computational mesh. Hence, studies with a higher number of repetitive numerical simulations may be

performed in 2-D computational domains, where the computational demand is relatively low.

- The effect of the gradient scheme in the discretization of the convective term is investigated, comparing the results obtained from the modified simulation with the ones obtained from the default scheme combination. Based on the results, the gradient scheme is effective on the overall results in terms of NMAE. The discretization of the compression flux is also investigated, and the interfaceCompression scheme is found to be a better option than the default linear scheme. However, the comparison between the interfaceCompression scheme and the combined effect of two schemes shows that the cell-limited gradient scheme decreases the peak pressure prediction performance.
- The effect of the discretization of the convective term is investigated for the momentum equation and the VOF-advection equation. The effects are examined in the momentum equation first, and then the VOF-advection equation is investigated using the best three results obtained in the former. There is no distinct numerical scheme that yields the best results in general, but some prominent results are obtained from the investigation depending on the focus. For the peak pressure prediction accuracy, the best scheme couple is the SuperBee on the momentum equation and the Gamma on the VOF-advection equation. On the other hand, if the limited linear scheme with a coefficient of 0.4 is applied to the momentum equation and the upwind scheme to the VOF-advection equation, the overall pressure prediction accuracy is significantly increased at the expense of peak pressure prediction accuracy. Another alternative scheme combination is the linear upwind coupled with the linear upwind scheme, which increases the performance of the overall results without decreasing the peak pressure prediction accuracy.
- The percent error obtained from the default scheme combination is 50.51%, which can be improved significantly using the SuperBee and Gamma combination to 0.5%, indicating a 99% improvement can be achieved with

this scheme combination. The default scheme combination for the overall pressure prediction results in an NRMSE of 0.2680 and an NMAE of 0.6372. These results can be reduced to 0.1739 and 0.3981 for the NRMSE and NMAE, respectively, which means the overall results can be improved up to 37.5% using the limited linear scheme with a coefficient of 0.4, combined with the upwind scheme. The SuperBee and Gamma scheme couple increases the computational time by 15%, while there is no significant effect on the computational time using the limited linear scheme with a coefficient of 0.4 coupled with the upwind scheme.

The investigation of numerical scheme performances on the prediction of impact pressures is attempted in this study. A couple of topics that arose during the investigations are left for future work:

- The investigation of the effect of divergence schemes showed that coupling numerical schemes regarding the momentum equation and the VOF-advection equation yields unique results for each couple. Therefore, each numerical scheme coupling option should be investigated, independent of the initial results obtained from the first step of the assessment of the VOF-advection equation discretization.
- The performance assessment is based on a physical experiment. The performance of the schemes should be investigated with different data sets.
- The investigation should be performed in studies in which the impact pressures are caused by regular and irregular waves, to come up with conclusions for the wave cases.
- Even though the flow is assumed to be laminar in the investigation, turbulent flow characteristics are involved after the impact. The investigation should also be performed using turbulence model.

REFERENCES

Arikawa, T., & Igarashi, H. (2018). Consideration on accuracy and computational efficiency of gas-liquid two-phase fluid simulation against Tsunami bore force (in Japanese). *Journal of Japan Society of Civil Engineers, Ser. B2 (Coastal Engineering), 74*(2). doi:10.2208/kaigan.74.i_1039

Berberović, E., van Hinsberg, N. P., Jakirlić, S., Roisman, I. V., & Tropea, C. (2009). Drop impact onto a liquid layer of finite thickness: Dynamics of the cavity evolution. *Physical Review E, 79*(3). doi:10.1103/physreve.79.036306

Bukreev, V. I., & Gusev, A. V. (2005). Initial Stage of the Generation of Dam-Break Waves. *Doklady Physics, 50*(4), 200-203. doi:10.1134/1.1922561

Bukreev, V. I., Gusev, A. V., Malysheva, A. A., & Malysheva, I. A. (2004). Experimental verification of the gas-hydraulic analogy with reference to the dam-break problem. *Fluid Dynamics, 39*(5), 801-809. doi:10.1007/s10697-005-0014-7

Chen, L., Taylor, P. H., Draper, S., & Wolgamot, H. (2019). 3-D numerical modelling of Greenwater loading on fixed ship-shaped FPSOs. *Journal of Fluids and Structures, 84*, 283-301. doi:10.1016/j.jfluidstructs.2018.11.003

Das, S. K., & Bagheri, J. (2015). Modelling of shallow-water equations by using compact MacCormack-Type schemes with application to dam-break problem. *International Journal of Advances in Applied Mathematics and Mechanics, 2*(3), 60-71.

Deshpande, S. S., Anumolu, L., & Trujillo, M. F. (2012). Evaluating the performance of the two-phase flow solver interFoam. *Computational Science & Discovery, 5*(1). doi:10.1088/1749-4699/5/1/014016

Dias, F., & Ghidaglia, J.-M. (2018). Slamming: Recent progress in the evaluation of impact pressures. *Annual Review of Fluid Mechanics, 50*(1), 243-273. doi:10.1146/annurev-fluid-010816-060121

Ferziger, J. H., Perić, M., & Street, R. L. (2020). *Computational methods for fluid dynamics* (4th ed.). Springer.

Glimm, J. (1965). Solutions in the Large for Nonlinear Hyperbolic Systems of Equations. *Communications on Pure and Applied Mathematics, 18*(4), 697-715. doi:10.1002/cpa.3160180408

Güler, H. G. (2020). Numerical Modelling of Wave-Structure Interaction Problems through CFD Methods (PhD. thesis). Middle East Technical University.

Hirt, C., & Nichols, B. (1981). Volume of fluid (VOF) method for the dynamics of Free Boundaries. *Journal of Computational Physics, 39*(1), 201-225. doi:10.1016/0021-9991(81)90145-5

Holzmann, T. (2016). *Mathematics, Numerics, Derivations and OpenFOAM.* www.holzmann-cfd.de.

Hu, C., & Kashiwagi, M. (2004). A CIP-based method for numerical simulations of violent free-surface flows. *Journal of Marine Science and Technology, 9*(4), 143-157. doi:10.1007/s00773-004-0180-z

Hu, C., & Sueyoshi, M. (2010). Numerical simulation and experiment on dam break problem. *Journal of Marine Science and Application, 9*(2), 109-114. doi:10.1007/s11804-010-9075-z

Jasak, H., Weller, H. G., & Gosman, A. D. (1999). High resolution NVD differencing scheme for arbitrarily unstructured meshes. *International Journal for Numerical Methods in Fluids, 31*(2), 431-449.

Ji, Q.-l., Zhao, X.-z., & Dong, S. (2013). Numerical study of violent impact flow using a CIP-based model. *Journal of Applied Mathematics, 2013*, 1-12. doi:10.1155/2013/920912

Kleefsman, K. M., Fekken, G., Veldman, A. E., Iwanowski, B., & Buchner, B. (2005). A volume-of-fluid based simulation method for wave impact problems. *Journal of Computational Physics, 206*(1), 363-393. doi:10.1016/j.jcp.2004.12.007

Lafeber, W., Brosser, L., & Bogaen, H. (2012). Elementary Loading Processes (ELP) involved in breaking wave impacts: findings from the Sloshel project. *The proceedings of the twenty-second (2012) International Offshore and polar engineering conference* (pp. 265-276). Rhodes, Greece: International Society of Offshore and Polar Engineers.

Lee, T.-h., Zhou, Z., & Cao, Y. (2002). Numerical simulations of hydraulic jumps in water sloshing and water impacting. *Journal of Fluids Engineering, 124*(1), 215-226. doi:10.1115/1.1436097

Leonard, B. P. (1979). A stable and accurate convective modelling procedure based on quadratic upstream interpolation. *Computer Methods in Applied Mechanics and Engineering, 19*(1), 59-98. doi:10.1016/0045-7825(79)90034-3

Lien, F. S., & Leschziner, M. A. (1994). Upstream monotonic interpolation for scalar transport with application to complex turbulent flows. *International Journal for Numerical Methods in Fluids, 19*(6), 527-548. doi:10.1002/fld.1650190606

Lobovský, L., Botia-Vera, E., Castellana, F., Mas-Soler, J., & Souto-Iglesias, A. (2014). Experimental investigation of dynamic pressure loads during dam break. *Journal of Fluids and Structures, 48*, 407-434. doi:10.1016/j.jfluidstructs.2014.03.009

Marsooli, R., & Wu, W. (2014). 3-D finite-volume model of dam-break flow over uneven beds based on VOF method. *Advances in Water Resources, 70*, 104-117. doi:10.1016/j.advwatres.2014.04.020

Mokrani, C., & Abadie, S. (2016). Conditions for peak pressure stability in VOF simulations of Dam Break Flow Impact. *Journal of Fluids and Structures, 62*, 86-103. doi:10.1016/j.jfluidstructs.2015.12.007

Moukalled, F., Mangani, L., & Darwish, M. (2016). *The finite volume method in Computational Fluid Dynamics: An advanced introduction with openfoam and MATLAB.* Springer.

OpenFOAM®. (2019). The Open-Source CFD Toolbox version 1912. OpenCFD Limited. http://www.openfoam.com.

Oumeraci, H., Allsop, W., Groot, M., Crouch, R., & Vrijling, J. (2001). Proverbs: Probabilistic design tools for vertical breakwaters.

Peng, L., Zhang, T., Rong, Y., Hu, C., & Feng, P. (2021). Numerical investigation of the impact of a dam-break induced flood on a structure. *Ocean Engineering, 223*, 1-15. doi:10.1016/j.oceaneng.2021.108669

Peregrine, D. H. (2003). Water-wave impact on walls. *Annual Review of Fluid Mechanics, 35*(1), 23-43. doi:10.1146/annurev.fluid.35.101101.161153

Roe, P. L. (1985). Some contributions to the modelling of discontinuous flows. *Lectures in Applied Mathematics, 22*, 163-193.

Roe, P. L. (1986). Characteristic-based schemes for the Euler equations. *Annual Review of Fluid Mechanics, 18*(1), 337-365. doi:10.1146/annurev.fl.18.010186.002005

Spalding, D. B. (1972). A novel finite difference formulation for differential expressions involving both first and second derivatives. *International Journal for Numerical Methods in Engineering, 4*, 551-559. doi:10.1002/nme.1620040409

Stansby, P. K., Chegini, A., & Barnes, T. C. (1998). The initial stages of dam-break flow. *Journal of Fluid Mechanics, 374*, 407-424. doi:10.1017/s0022112098001918

Sweby, P. K. (1984). High resolution schemes using flux limiters for hyperbolic conservation laws. *SIAM Journal on Numerical Analysis, 21*(5), 995-1011. doi:10.1137/0721062

van Albada, G. D., van Leer, B., & Roberts, W. W. (1982). A comparative study of computational methods in Cosmic Gas Dynamics. *Astronomy and Astrophysics, 108*, 76-84.

van Leer, B. (1974). Towards the ultimate conservative difference scheme. II. Monotonicity and conservation combined in a second-order scheme. *Journal of Computational Physics, 14*(4), 361-370. doi:10.1016/0021-9991(74)90019-9

van Leer, B. (1977). Towards the ultimate conservative difference scheme. IV. A new approach to numerical convection. *Journal of Computational Physics, 23*(3), 276-299. doi:10.1016/0021-9991(77)90095-x

van Leer, B. (1979). Towards the ultimate conservative difference scheme. V. A second-order sequel to Godunov's method. *Journal of Computational Physics, 32*(1), 101-136. doi:10.1016/0021-9991(79)90145-1

Warming, R. F., & Beam, R. M. (1976). Upwind second-order difference schemes and applications in aerodynamic flows. *AIAA Journal, 14*(9), 1241-1249. doi:10.2514/3.61457

Waterson, N. P., & Deconinck, H. (2007). Design principles for bounded higher-order convection schemes – a unified approach. *Journal of Computational Physics, 224*(1), 182-207. doi:10.1016/j.jcp.2007.01.021

Wemmenhove, R., Gladsø, R., Iwanowski, B., & Lefranc, M. (2010). Comparison of CFD Calculations and Experiment for the Dambreak Experiment with One Flexible Wall. *Proceedings of the Twentieth (2010) International Offshore and Polar Engineering Conference* (pp. 200-205). Beijing, China: ISOPE.

Zhang, T., Fang, F., & Feng, P. (2017). Simulation of dam/levee-break hydrodynamics with a three-dimensional implicit unstructured-mesh finite element model. *Environmental Fluid Mechanics, 17*(5), 959-979. doi:10.1007/s10652-017-9530-3

Zhou, Z., de Kat, J., & Buchner, B. (1999). A nonlinear 3-D approach to simulate green water dynamics on deck.

Ziman, H. J. (1990). Computer Prediction of Chemically Reacting Flows in Stirred Tanks (PhD. Thesis). Imperial College of Science, Technology and Medicine.

APPENDICES

A. Results of the Effect of the Discretization of the Convective Terms in Momentum Equation

Table 5.1. Results of the effect of the discretization of convective terms in momentum equation

Cases	PE Sensor-1	PE Sensor-2	PE Sensor-3	PE Sensor-4	NRMSE Sensor-1	NRMSE Sensor-2	NRMSE Sensor-3	NRMSE Sensor-4	NMAE Sensor-1	NMAE Sensor-2	NMAE Sensor-3	NMAE Sensor-4
linear	3.90%	12.51%	2.16%	55.29%	0.2055	0.2885	0.2595	0.6722	0.5100	0.4942	0.4765	0.8581
midpoint	4.37%	12.79%	1.97%	56.60%	0.2043	0.2881	0.2632	0.6708	0.5110	0.4915	0.4821	0.8591
upwind	18.27%	0.66%	13.98%	59.19%	0.3191	0.2855	0.2926	0.7094	0.6303	0.4343	0.4523	0.7604
linear upwind	26.63%	12.33%	10.47%	56.33%	0.2688	0.2742	0.2337	0.6194	0.3411	0.3731	0.3926	0.7182
limited linear 0.2	12.17%	5.14%	9.11%	58.27%	0.2463	0.3435	0.2788	0.7004	0.5010	0.4603	0.4457	0.7648
limited linear 0.4	3.22%	1.81%	9.07%	57.67%	0.2431	0.3324	0.2761	0.7039	0.4911	0.4478	0.4452	0.7511
limited linear 0.6	24.01%	1.45%	9.64%	57.85%	0.2277	0.3403	0.2763	0.6999	0.4747	0.4485	0.4445	0.7616
limited linear 0.8	20.99%	1.84%	6.96%	58.58%	0.2392	0.3394	0.2750	0.7008	0.4744	0.4417	0.4385	0.7588
limited linear 1	17.33%	0.29%	6.96%	58.37%	0.2464	0.3322	0.2709	0.7011	0.4679	0.4298	0.4340	0.7594
Minmod	9.78%	2.22%	10.24%	59.98%	0.2511	0.3010	0.2586	0.7078	0.4599	0.3964	0.4149	0.7658
MinmodV	21.84%	9.43%	8.83%	59.45%	0.2751	0.2850	0.2558	0.6900	0.4792	0.3821	0.4094	0.7505
vanLeer	15.96%	2.79%	6.91%	55.92%	0.2038	0.2927	0.2588	0.6892	0.3871	0.3794	0.4108	0.7522
vanLeerV	21.95%	10.90%	10.59%	59.73%	0.2751	0.2864	0.2572	0.6892	0.4487	0.3816	0.4117	0.7556
MUSCL	14.58%	7.59%	1.15%	55.13%	0.2275	0.3189	0.2894	0.6787	0.4302	0.4271	0.4465	0.7625
MUSCLV	21.61%	11.98%	8.43%	58.07%	0.2676	0.2852	0.2584	0.6855	0.4221	0.3758	0.4140	0.7572
QUICK	27.27%	19.00%	8.30%	51.54%	0.2609	0.3392	0.2867	0.6460	0.4961	0.4824	0.4890	0.8286
QUICKV	25.92%	6.10%	7.45%	56.77%	0.2213	0.3070	0.2770	0.6595	0.4369	0.4271	0.4727	0.8577
UMIST	20.56%	4.84%	5.35%	57.38%	0.2301	0.2852	0.2581	0.6849	0.4001	0.3654	0.4128	0.7445
UMISTV	22.02%	10.54%	9.94%	59.13%	0.2785	0.2864	0.2567	0.6884	0.4567	0.3835	0.4112	0.7569
vanAlbada	7.91%	2.92%	9.70%	58.82%	0.2329	0.2906	0.2537	0.7058	0.4203	0.3749	0.4070	0.7670
vanAlbadaV	21.88%	11.49%	8.66%	59.25%	0.2784	0.2846	0.2568	0.6908	0.4665	0.3806	0.4101	0.7522
SuperBee	5.10%	7.82%	2.02%	48.94%	0.1891	0.3020	0.2568	0.6345	0.4095	0.3917	0.4023	0.6842
SuperBeeV	23.17%	12.25%	5.52%	59.55%	0.2542	0.2868	0.2522	0.6695	0.3849	0.3999	0.4115	0.7954
SFCD	19.76%	2.93%	9.77%	59.67%	0.2173	0.2931	0.2551	0.7069	0.4445	0.3886	0.4132	0.7666
SFCDV	23.32%	10.06%	8.81%	59.13%	0.2823	0.2851	0.2552	0.6902	0.4841	0.3833	0.4107	0.7531
Gamma	20.67%	1.59%	9.35%	60.86%	0.2076	0.2933	0.2565	0.7029	0.4347	0.3895	0.4156	0.7628
GammaV	22.93%	10.76%	8.68%	58.92%	0.2783	0.2860	0.2568	0.6865	0.4777	0.3866	0.4156	0.7533

B. Results of the Effect of the Discretization of the Convective Terms in VOF-Advection Equation

Table 5.2. Results of the effect of the discretization of convective terms in VOF-advection equation with limited linear scheme with a coefficient of 0.4 is applied to momentum equation

Cases	PE Sensor-1	PE Sensor-2	PE Sensor-3	PE Sensor-4	NRMSE Sensor-1	NRMSE Sensor-2	NRMSE Sensor-3	NRMSE Sensor-4	NMAE Sensor-1	NMAE Sensor-2	NMAE Sensor-3	NMAE Sensor-4
linear	18.83%	9.34%	12.47%	58.71%	0.2769	0.3321	0.2808	0.7058	0.4567	0.4257	0.4503	0.7304
midpoint	18.79%	9.28%	12.57%	58.31%	0.2772	0.3319	0.2817	0.7046	0.4575	0.4258	0.4514	0.7273
upwind	14.11%	6.28%	13.30%	59.86%	0.1739	0.2708	0.2731	0.7038	0.3981	0.3926	0.4514	0.7299
linear upwind	17.66%	3.57%	7.83%	57.53%	0.2442	0.3253	0.2719	0.6954	0.4775	0.4362	0.4328	0.7550
limited linear 0.2	8.28%	0.30%	7.91%	58.49%	0.2477	0.3071	0.2593	0.7077	0.4510	0.3944	0.4220	0.7278
limited linear 0.4	2.29%	2.02%	9.40%	58.74%	0.2136	0.3069	0.2618	0.7059	0.4443	0.3977	0.4238	0.7316
limited linear 0.6	8.48%	1.55%	10.36%	58.18%	0.2092	0.3040	0.2594	0.7042	0.4491	0.4022	0.4226	0.7390
limited linear 0.8	8.50%	0.84%	10.56%	58.36%	0.2063	0.3043	0.2616	0.7072	0.4469	0.4005	0.4238	0.7352
limited linear 1	8.37%	0.19%	11.29%	57.91%	0.2051	0.3048	0.2625	0.7062	0.4463	0.4005	0.4233	0.7318
Minmod	8.21%	1.36%	11.86%	59.41%	0.2220	0.3024	0.2631	0.7105	0.4528	0.3984	0.4258	0.7217
vanLeer	3.22%	1.81%	9.07%	57.67%	0.2431	0.3324	0.2761	0.7039	0.4911	0.4478	0.4452	0.7511
MUSCL	19.31%	6.01%	9.67%	58.23%	0.2669	0.3066	0.2711	0.6853	0.5129	0.4288	0.4308	0.7384
QUICK	15.31%	5.43%	9.96%	58.90%	0.2496	0.3057	0.2655	0.6917	0.4433	0.4061	0.4223	0.7418
UMIST	9.09%	4.32%	12.57%	57.68%	0.2312	0.3241	0.2772	0.6931	0.4794	0.4411	0.4461	0.7537
vanAlbada	3.51%	0.18%	11.00%	59.79%	0.2299	0.3171	0.2656	0.7062	0.4681	0.4150	0.4304	0.7352
SuperBee	32.43%	14.06%	9.50%	58.47%	0.2887	0.2981	0.2646	0.6820	0.5286	0.4168	0.4212	0.7357
SFCD	4.79%	0.70%	11.68%	59.44%	0.2102	0.3158	0.2684	0.7051	0.4455	0.4166	0.4351	0.7252
Gamma	3.54%	2.01%	13.06%	60.13%	0.2055	0.3161	0.2678	0.7061	0.4380	0.4177	0.4352	0.7236

Table 5.3. Results of the effect of the discretization of convective terms in VOF-advection equation with SuperBee scheme is applied to momentum equation

Cases	PE Sensor-1	PE Sensor-2	PE Sensor-3	PE Sensor-4	NRMSE Sensor-1	NRMSE Sensor-2	NRMSE Sensor-3	NRMSE Sensor-4	NMAE Sensor-1	NMAE Sensor-2	NMAE Sensor-3	NMAE Sensor-4
linear	24.25%	4.22%	7.08%	46.51%	0.2495	0.2575	0.1922	0.5569	0.3502	0.3224	0.2993	0.6210
midpoint	19.72%	5.22%	5.79%	48.79%	0.2310	0.2475	0.1889	0.5764	0.3341	0.3219	0.2761	0.6155
upwind	9.22%	5.44%	1.21%	55.44%	0.2700	0.2702	0.2580	0.6079	0.5073	0.4093	0.4066	0.6404
linear upwind	44.87%	15.30%	15.59%	51.92%	0.2520	0.2946	0.2570	0.6134	0.4205	0.3580	0.3771	0.6582
limited linear 0.2	23.46%	9.34%	5.78%	52.67%	0.2091	0.2707	0.2082	0.6207	0.3541	0.3723	0.3486	0.6947
limited linear 0.4	23.27%	2.16%	3.44%	45.33%	0.2367	0.2735	0.2043	0.6063	0.3970	0.3632	0.3345	0.5907
limited linear 0.6	37.12%	0.51%	7.66%	45.53%	0.2195	0.2896	0.2284	0.5895	0.4000	0.3357	0.3455	0.6228
limited linear 0.8	43.03%	0.75%	2.13%	47.54%	0.2480	0.2958	0.2374	0.5876	0.3449	0.3172	0.3754	0.6744
limited linear 1	49.04%	10.95%	0.81%	46.56%	0.2160	0.3148	0.2509	0.6250	0.3751	0.3731	0.3907	0.6529
Minmod	5.70%	4.44%	14.76%	52.43%	0.2147	0.2640	0.2327	0.6260	0.3562	0.3548	0.3707	0.6176
vanLeer	5.10%	7.82%	2.02%	48.94%	0.1891	0.3020	0.2568	0.6345	0.4095	0.3917	0.4023	0.6842
MUSCL	27.10%	38.07%	5.79%	40.06%	0.2297	0.2921	0.2439	0.5851	0.4167	0.3753	0.3601	0.6341
QUICK	59.62%	21.74%	11.66%	44.96%	0.3008	0.3565	0.1956	0.5781	0.4886	0.3648	0.2719	0.5489
UMIST	71.28%	28.42%	5.36%	44.32%	0.2480	0.3309	0.2349	0.6361	0.4916	0.4323	0.4041	0.6451
vanAlbada	49.24%	17.60%	0.38%	54.26%	0.2888	0.3236	0.2230	0.5878	0.4197	0.3418	0.3563	0.6616
SuperBee	37.83%	48.76%	22.43%	45.79%	0.2110	0.2860	0.2389	0.5893	0.4194	0.3988	0.3693	0.6946
SFCD	16.88%	14.32%	1.72%	43.62%	0.2054	0.2359	0.2489	0.6117	0.3874	0.3529	0.3710	0.6754
Gamma	0.50%	2.97%	2.64%	42.31%	0.2217	0.2545	0.2127	0.6097	0.3322	0.2953	0.3195	0.5934

Table 5.4. Results of the effect of the discretization of convective terms in VOF-advection equation with linear upwind scheme is applied to momentum equation

Cases	PE Sensor-1	PE Sensor-2	PE Sensor-3	PE Sensor-4	NRMSE Sensor-1	NRMSE Sensor-2	NRMSE Sensor-3	NRMSE Sensor-4	NMAE Sensor-1	NMAE Sensor-2	NMAE Sensor-3	NMAE Sensor-4
linear	24.87%	17.24%	8.22%	56.15%	0.2600	0.2774	0.2601	0.6225	0.3212	0.3721	0.4220	0.6871
midpoint	24.92%	17.17%	7.93%	56.06%	0.2605	0.2776	0.2597	0.6229	0.3221	0.3726	0.4209	0.6868
upwind	18.25%	6.18%	9.44%	58.31%	0.1818	0.2842	0.2878	0.6465	0.3343	0.3711	0.4421	0.6664
linear upwind	2.77%	17.49%	7.67%	56.42%	0.2404	0.2742	0.2413	0.6221	0.3349	0.3611	0.3928	0.6959
limited linear 0.2	16.11%	3.73%	8.69%	56.32%	0.2514	0.2674	0.2294	0.6175	0.3065	0.3501	0.3795	0.6922
limited linear 0.4	16.41%	5.44%	9.42%	55.82%	0.2557	0.2786	0.2308	0.6123	0.3193	0.3677	0.3862	0.7192
limited linear 0.6	16.24%	2.32%	8.18%	56.39%	0.2596	0.2806	0.2334	0.6118	0.3227	0.3705	0.3917	0.7314
limited linear 0.8	15.58%	1.51%	8.52%	56.02%	0.2574	0.2837	0.2355	0.6183	0.3268	0.3731	0.3909	0.7189
limited linear 1	15.14%	1.31%	8.38%	56.95%	0.2573	0.2855	0.2344	0.6161	0.3268	0.3807	0.3905	0.7308
Minmod	11.85%	2.53%	8.86%	55.95%	0.2522	0.2853	0.2390	0.6225	0.3343	0.3827	0.3911	0.7125
vanLeer	26.63%	12.33%	10.47%	56.33%	0.2688	0.2742	0.2337	0.6194	0.3411	0.3731	0.3926	0.7182
MUSCL	34.37%	20.39%	7.34%	57.78%	0.2802	0.2811	0.2348	0.6184	0.3651	0.3872	0.3954	0.7124
QUICK	27.45%	25.30%	9.29%	56.31%	0.2733	0.2903	0.2487	0.6173	0.3371	0.3912	0.4053	0.7288
UMIST	29.05%	13.65%	10.28%	57.22%	0.2677	0.2716	0.2326	0.6221	0.3389	0.3684	0.3914	0.7154
vanAlbada	15.43%	4.96%	7.25%	56.25%	0.2565	0.2848	0.2430	0.6277	0.3440	0.3855	0.4013	0.7023
SuperBee	36.56%	21.45%	8.61%	57.62%	0.2924	0.2859	0.2387	0.6225	0.4119	0.3859	0.3816	0.6944
SFCD	11.94%	12.23%	10.29%	56.67%	0.2550	0.2967	0.2590	0.6308	0.3773	0.4098	0.4240	0.7001
Gamma	13.10%	13.28%	9.91%	56.66%	0.2557	0.2990	0.2564	0.6258	0.3747	0.4186	0.4205	0.7123